April 2021

Investigation of CoO ATO for Solar Cells and Infrared Sheaths

Manopriya Devisetty Subramanyam
University of South Florida

Investigation of CoO ATO for Solar Cells and Infrared Sheaths

by

Manopriya Devisetty Subramanyam

A dissertation submitted in partial fulfillment
of the requirements for the degree of
Doctor of Philosophy
Department of Electrical Engineering
College of Engineering
University of South Florida

Major Professor: Sylvia Thomas, Ph.D.
Arash Takshi, Ph.D.
Andrew Hoff, Ph.D.
Theresa Evans Nyugen, Ph.D.
Scott Campbell, Ph.D.

Date of Approval:
Dec 3, 2020

Dedication

This work is dedicated to my parents and husband.

Table of Contents

List of Tables

List of Figures

Abstract

Solar as an energy source is expected to grow fastest from now to 2050. Increasing the efficiency is usually achieved by increasing the short circuit current density (J_{SC}) and/or the fill factor. Improving the efficiency of solar cells will be an ongoing effort.

Structurally solar technologies can be classified into two types, wafer-based and thin-film-based. Wafer solar cells have been used in this study. The anti-reflective layer on top of solar cells has been fabricated by a process called electrospinning to tune the solar cells' top surface with the desired thickness and dimensions of the nanofibers. The nanofibers' dimensions, shape, and alignment are tuned by changing the precursor solution's concentration, changing the fabrication parameters such as the 1. Voltage between needle tip and collector plate 2. Distance between needle tip and collector plate and 3. The flow rate of solution in the syringe pump.

Physical or structural properties have been studied by using Scanning Electron Microscopy (SEM), Electron Dispersive Microscopy (EDS), Atomic Force Microscopy (AFM). Electrical characterization was carried out using a short circuit current- Voltage (J-V) and multimeter measurements.

Chapter 1: Introduction

We need to power our planet for many decades to come. Green energy practices need to be developed and practiced. Solar cells convert sunlight into energy. This sunlight is free of cost and is abundant, at least in most places. Currently, 2.58% of the total electricity generated by the United States is solar energy. One of the reasons for a low percentage is the relatively high cost per watt of generation. The fabrication of solar cells drives up the cost per watt. If any part of the process can be simplified without rigorous fabrication, the process must be adapted.

Electromagnetic waves of infrared wavelengths are used in technologies like sensors and imaging. Infrared imaging enables us to detect various objects in the dark and image objects that are very far away. In aviation, infrared imaging is used to track jet aircraft and helicopters using IRST (Infrared Sighting and Tracking) [1], offering a certain level of security. An infrared camera detects and picks up the infrared wavelengths and processes it into an image. Infrared technology is also used in fault and leak detection of machinery as a non-destructive method of testing.

All objects that are at a temperature above 0K (zero Kelvin) emit IR (infrared radiation). Most of this IR is absorbed by water vapor, dust particles, carbon dioxide molecules from the atmosphere [2] [3]. Stefan-Boltzmann's law states that IR radiation intensity is proportional to the fourth power of the objects' surface temperature. The equation is given below.

$$E = \sigma T^4$$

$$\sigma = 8.670374419 * 10^{-8} \, Wm^{-2}K^{-4}$$

where σ is the Stefan Boltzmann constant, for specific military applications, being undetected by infrared detectors may be favorable. This is called stealth technology. Therefore, to

normalize the IR emitted to the ambient surroundings, an adequate sheath needs to be used. For the object to be undetected by an IR imaging device, the object needs to be coated with an insulating material that does not allow the inner heat to reach the surface, thus keeping the surface temperature similar to the ambient temperature. Metals, metal oxides, semiconductors, and conducting polymers are good at IR shielding. [4] [5] [6] [7]. Some outdoor devices and aerospace vehicles may benefit from an infrared coating so that damage due to infrared waves may be minimized, thereby promoting the devices' longevity.

Solar cells are PN junction devices. When incident photons from the sun are absorbed in the solar cell, electron-hole pairs are created. When an external load is connected or short-circuited, the light-induced charge carriers to flow through the external circuit. Quantum efficiency is the ratio of the number of charge carriers generated to the number of photons for a given energy. Quantum energy can be a function of wavelength or energy. This work will investigate infrared-reflective material for the capability of reflecting infrared wavelengths.

This dissertation reports on CoO (Cobalt Oxide) and ATO (Antimony doped Tin Oxide) as innovative materials for device technology as 1) anti-reflecting coatings (membranes) on solar cells and 2) super elastic infrared sheaths (membranes).

1.1. Outline

Outline for the dissertation is as follows. Chapter one introduces the concepts of reflectivity, infrared sheath, and solar cells. Chapter two elaborates on the materials of choice. Chapter three is a description of electrospinning as a fabrication process. Chapter four is the study of Cobalt Oxide (CoO) and Antimony doped Tin Oxide (ATO) electrospun nanofiber membrane as the anti-reflective layer or the top layer of a solar cell. Chapter five is the study of fabricating a highly

elastic infrared reflecting membrane. Chapter six is a summary of findings. Chapter seven concludes the work and some possible future work is discovered.

1.2. Background

1.2.1. Solar Spectrum

Solar cells convert photons from solar radiation or solar energy into electrical energy. These photons incident on the solar cell are absorbed into the material to generate charge carriers, i.e., the electron-hole pairs. These electrons pass through an external load in the form of a load current. The load current is the electrical energy generated. Photovoltaic devices are in a wide variety of commercial products: simple do-it-yourself kits, toys, calculators, to solar fields that generate up to a few megawatts. The largest to date is a 2245 MW_{DC} at Bhadla Solar Park in India [8]. There are several small-scale generation systems in use as well (1kW).

The spectrum of solar energy from the sun comes in electromagnetic irradiation over a broad spectrum. The longer the wavelength of electromagnetic radiation, the smaller the energy; the shorter the wavelength, the higher the energy.

The irradiation emitted by the sun has a spectrum that is similar to black body radiation at around 6000 K to 7000 K. Two main irradiation spectrums have been decided as the standard. They are AM0 and AM1.0; AM stands for Air Mass. AM1.0 is the spectrum that represents when the sun is located directly above that location, i.e., the shortest path through the atmosphere, taking into account the scattering effects of the earth's atmosphere and on the atmosphere composition. Measurements in AM 0 are taken to simulate satellites' radiation spectrum where there is no atmosphere. The value of AM 0 is 1.353 kWm^{-2}. AM 1.0 is 1 kWm^{-2}. The energy loss is due to the absorption of wavelengths by molecules in the atmosphere, air, humidity or water vapor, dust etc. Scattering decreases the intensity of the spectrum and causes the light to arrive at random

directions called diffused light. The increased surface area of the top anti-reflecting layer helps transmit more diffused light into the solar cell.

1.2.2. Refractive Index

A Refractive index is a measure of the speed of light in a medium.

$$n = \frac{c}{v}$$

where c is the speed of light, v is the phase velocity in the medium

1.2.3. Snells Law

Snell's law relates the angles of incidence and refraction to the refractive indices of the media.

$$n_1 \sin \theta_1 = n_2 \sin \theta_2$$

when the $n_1 > n_2$, the transmitted angle is greater than the incidence angle. The incidence angle is called the critical angle θ_c

Where,

$$\sin \theta_c = \frac{n_2}{n_1}$$

When the incidence angle θ_i exceeds θ_c, there is no transmitted wave. We see only reflected waves. The latter phenomenon is called the total internal reflection (TIR).

Total Internal Reflection (TIR) is the effect of increasing the incidence angle. TIR phenomenon leads to propagating waves in a dielectric medium surrounded by a medium of smaller refractive indices. By Snell's law, the two layers' refractive indices at the interface determine the amount of light transmitted or reflected.
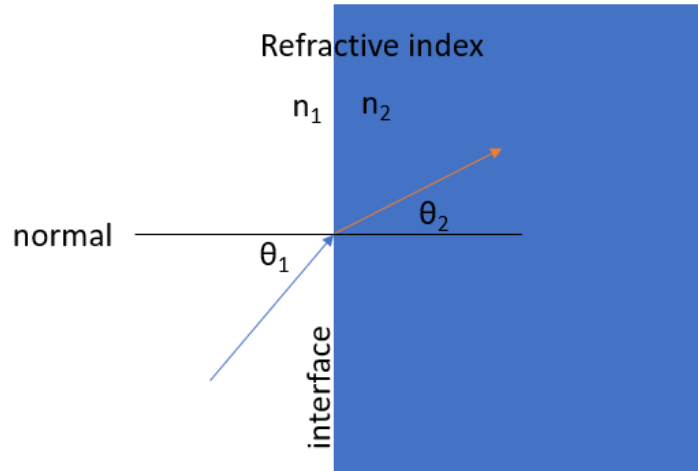
Figure 1: Snell's law

For the past 30 years, solar cells have been studied extensively as a renewable energy source or clean energy. Many forms of solar cells have been explored (thin-film solar cells, dye-sensitized solar cells, monocrystalline solar cells, multi-junction solar cells, plasmonic solar cells, quantum dot solar cells, hybrid solar cells, biohybrid solar cells). Constant effort is put into making solar cells more efficient. Commercial solar cells show efficiency of around 12% to 16%. Increasing the efficiencies by a few percent is a considerable improvement [9].

1.2.4. Thermal Radiation Equations

Weins law relates the maximum wavelength (λ_{max}) of radiation from a body to its temperature (T). $3 * 10^7$ is the constant of proportionality.

$$\lambda_{max} = \frac{3 * 10^7}{T}$$

Stefan Boltzmann's law states that IR radiation intensity is proportional to the fourth power of the objects' fourth power of the object's surface temperature. This law is a phenomenological description of the energy radiated (as electromagnetic waves) from a surface per second. When a surface is heated to a temperature T, it radiates net energy at a rate given by E

$$E = \sigma T^4$$

5

$$\sigma = 5.670374419 * 10^{-8} \, Wm^{-2}K^{-4}$$

Luis De Broglie discovered a relationship between energy and the speed of light. A constant called Planck's constant represents the relation between momentum and wavelength of a photon. The energy of a photon can be calculated from its frequency.

$$E = h * v = h\left(\frac{c}{\lambda}\right)$$

where h is the Planck's constant, v is the velocity of light, which can also be given as,

$$v = \left(\frac{c}{\lambda}\right)$$

An anti-reflective coating reduces losses due to reflectance and enhances the efficiency of solar cells. Anti-reflective coatings are based on interference of light from two or more interfaces. An anti-reflective coating is chosen such that the refractive index is between the refractive indices of the two media. Sometimes more than one layer of anti-reflective coatings is used to increase the bandwidth and angular tolerance. [10]

These coatings are used on optical devices, optical data storage. It is a flat or patterned dielectric layer with a refractive index between air and the devices' active materials. [11, 12]. Different structures like slits, squares and hexagon, pyramid, rods, cubes, etc., have been studied as anti-reflecting coatings [13] [14].

Recently applications of nanofibers in optical research have gained attention. Nanofiber membranes exhibit excellent characteristics such as increased piezoelectricity, hydrophobicity and so on [15]. Nanofiberfilms can exhibit high scattering based on Mie's theory [16]. There are many methods of Fabricating thin films or membranes. Spin coating, dip coating, CVD- chemical vapor deposition, electrospray deposition, dual solvent technique, etc., are major ways to fabricate thin films. Some researchers are also studying anti-reflective coatings that mimic the compound eyes of insects like moths. These structures were investigated on GaInP/GaInA PV modules, and an

improved current density was noted. Such complex omnidirectional structures have shown an in=mproved AR efficiency over a wide range of light incidence angles. [17, 18, 19].

There are many ways to fabricate nanofibers. They are as follows: self assembly [20] [21], melt blowing [22] [23], ultrasonic blowing [24, 25], solution blowing [26] [27], direct blow spinning [28] [29] and electrospinning [15] [30]. Electrospinning is the most effective, quick way of fabricating nanofibers. This process is widely accepted in academics as well as industrial applications. Electrospun fibers have been adopted since they are tunable structures, simple chemical modifications, abundant pores etc.

1.2.5. Structure of Solar Cells

The solar cell structure is as follows (Figure 2): from the top- ARC (Anti-reflective Coating), N-type semiconductor, P-type semiconductor, and lowest is aluminum oxide. The top ARC layer is to maximize the intensity of light waves entering the solar cell. A material having high transmittance and low absorption, and low reflectivity is chosen as an ARC. When the photon enters past the ARC into the semiconductor, an electron-hole pair is generated. The hole moves into the p-type material and recombines with the electron entering from the external load. The electron generated in the n-type material passes through the external load, causing a current to flow. All photons entering the solar cell are not converted into an electron-hole pair. Some photons traverse the thickness of the cell without generating an electron-hole pair. A mirror or a reflective coating is deposited on the bottom of the solar cell to avoid loss of these photons.

As the n side is narrow, most photons are absorbed in the depletion region and p side. The generated electron-hole pair are immediately separated by the built-in electric field E_0, which drifts them apart. The electron drifts and reaches the n side, making this region negative by an amount of charge, e. Similarly, the hole drifts and reaches the p side making this side positive.

Subsequently, the open-circuit voltage develops between the terminals of the device with the p side positive concerning the n side. When an external load is connected, the electron on the n side can travel around the external circuit and reach the p side to recombine with the excess hole. It should be noted that without the internal field E_0, the photogenerated electron-hole pair can't drift apart.
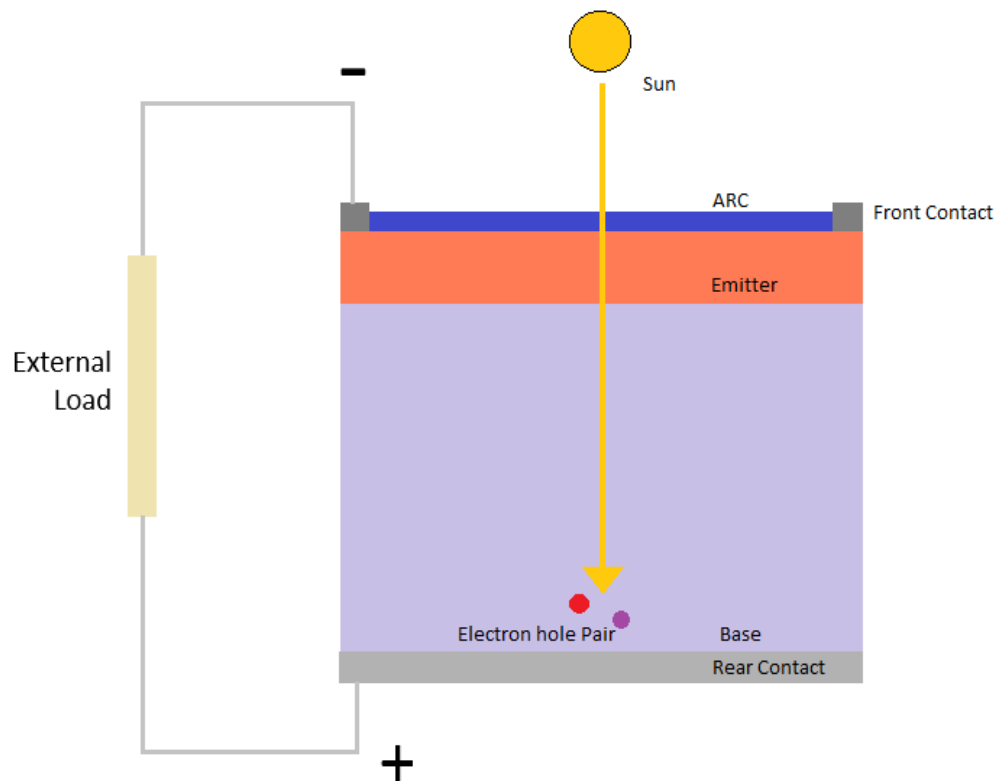
Figure 2: Structure of a solar cell connected to an external load

Under steady-state operation, there can be no net current through an open circuit of the solar cell. The photocurrent inside the solar cell due to the flow of photogenerated carriers must be balanced by a flow of carriers in the opposite direction. These are the minority carriers formed when a photovoltaic voltage across the p-n junction as in a normal diode. Electron hole pairs

generated by low wavelength or high energy photons are absorbed in the n side near the surface region or outside of the diffusion length to the depletion region. These electron-hole pairs are lost as the n-type region is heavily doped; these electron-hole pairs are lost by recombination. This is the reason why n-type is made very thin, usually around 200 nm. N-type is usually shorter than the p-type region.

Monocrystalline silicon has a bandgap of 1.1 eV, which translates to a 1.1 micrometer wavelength of electromagnetic radiation (Infrared). The incoming energy from solar rays with a greater wavelength than 1.1 micrometers is wasted, which is not a small amount. It is approximately 25 percent of the incoming solar radiation. The higher energy or the shorter wavelength of light can not produce electron-hole pairs as the electron-hole pairs are generated near the surface and lost by recombination. Loss can be as high as 40 percent. These two combined bring down the efficiency to less than 45 percent. When the antireflection coating is not perfect, it reduces the factor of electrons being collected by .8 or .9. Another constraint is the photovoltaic performance of the device itself. The upper limit of solar cells built on a monocrystalline silicon wafer has the maximum efficiency of 26% at room temperature. The efficiency of polycrystalline is around 12 to 19 percent. Amorphous crystalline solar cells have an efficiency of 8 to 13 percent.

Leem. J et al. [31] reported a 17% efficiency increase from an ATO film solar cell to a bare cell. Also, a 26% increase in efficiency of a bare solar cell to a nano ATO layer solar cell.

1.2.6. Anti-reflective Coatings for Solar Cells

A factor that inhibits light from entering the solar cell is reflection. While designing a solar cell, measures are taken to prevent reflection. Some methods include CVD (Chemical Vapor Deposition, patterning by etching down the top glass layer into micro or nanostructures, spin coating the solar cell, PECVD- Plasma Enhanced Chemical Vapor Deposition etc. Some common

antireflecting coatings are silicon nitride, titanium dioxide [32], aluminum oxide [33], tantalum oxide [34].

The fabrication of solar cells by itself may get a byproduct of Phosphorus Silicate Glass (PSG). This PSG also is anti-reflecting to an extent [35]. But since better materials are available as an anti-reflective coating, PSG is stripped by hydrogen fluoride. The choice of materials and the corresponding thickness should be made. If a thicker ARC layer is deposited, it negatively affects the solar cell by not letting enough light t pass through to the solar cell's active region.

1.3. Hypothesis

1. It is hypothesized that the chosen antimony doped tin oxide (ATO, $Sb-SnO_2$) and cobalt oxide (CoO) materials can exhibit desired optical properties and infrared reflectivity as electrospun nanofiber membranes.

2. It is hypothesized that a CoO ATO anti-reflective membrane coating using a targeted weight-to-weight composition can increase the current density of a solar cell.

3. It is hypothesized that a composite of CoO ATO and a super elastic polyimide will demonstrate favorable properties for a flexible infrared sheath.

1.4. Objectives

1. To fabricate, characterize, test, and analyze a CoO-ATO anti-reflective membrane coating for a solar cell.

2. To fabricate, characterize, test, and analyze a super elastic polyimide infrared reflecting membrane.

Chapter 2: Materials

Various metal oxide composites have been studied for applications in the military, energy harvesting, and optical arenas. These materials have diverse characteristics that make them attractive for use as anti-reflective coatings, protective membranes, and infra-red sheaths [36, 37, 38]. For example, composites of carbon fibers have been used to reinforce metal castings used in the body of airplanes [39], impacting the weight and agility of the aircraft [40, 41, 3]. Enhancement of these carbon fibers was reported by Richard et al. [3]. To further mitigate the threat to military aircraft being subject to laser attacks, Richard et al. developed a thermally reflective sol-gel coating of cobalt-oxide doped ATO (x% CoO, where .2<x<.5) for carbon fiber mats. As a transparent conducting oxide (TCO), CoO-ATO sol-gel used as a coating for carbon fiber mats demonstrated hemispherical reflectance in the IR region and angular dependency of reflectance. In addition, this material composite of CoO-ATO sol-gel was reported as a thermo-responsive dopant and surface heat dissipating material [3]. These CoO-ATO sol-gel coatings offer IR thermal reflectivity for wavelengths of 0.7-1.2 μm and show enhanced optical properties when altering the percentage of CoO in the composite. As thin film coatings, these composites are limited in the versatility of their applications and could benefit from investigative research surrounding the fabrication of these materials as nanostructures.

2.1. Transparent Conducting Oxide

Transparent Conducting Oxide (TCO) is a name given to a few oxides that are unusually transparent as most oxides of metals are not transparent. Some of the TCOs are Zinc Oxide (ZnO) and Tin Oxide (SnO). TCOs, unlike most oxides, are electrically conducting.

Table 1: Comparison of anti reflecting coatings [3, 15, 42, 43, 44, 45, 46, 47]

Properties	ATO	Cr_2O_3 (undoped)	TiO_2 (undoped)
Optimal Annealing Temperature (K)	723	873	673
Band Gap Energy (eV)	~3.6	~3.4	3.0 – 3.2
Reflectivity Spectral Range (nm)	620-640	2500 - 2600	388 - 413
Heat Treatment Range	450-550	350-400	400-450
Beneficial Parameters	Mid and far-range infrared reflectivity, resistant to oxidation, bandgap controlled by heat treatment and doping level.	2435 K melting temperature., oxidative resistant[1], mid-range infrared reflectivity	Near and mid-range infrared reflectivity, bandgap controlled by heat treatment

Tin oxide is an n-type semiconductor. It has a wide bandgap of 3.6 eV. For this reason, tin oxide is used in solar devices, sensor applications, heating elements in aircraft, automobile windows for defogging, and transparent electrodes in display technologies [48]. Tin oxide (SnO_2) crystalline structure is called a rutile structure. The conductivity is controlled by dopin. ATO, ITO (Indium Tin Oxide), and FTO (Fluorine Tin Oxide) are the common doped tin oxides. Antimony is an n-type donor. When tin oxide is doped with antimony, it is electrically conducting. The

increase in electrical conductivity is due to the formation of Sb5+ energetic levels overlapping the bottom of the conduction band. [49]

2.1.1. Antimony Tin Oxide

The properties of ATO: Low resistivity (~10-3 Ohm cm), Optically transparent (> 80%), Infrared reflecting, Hardness (Mohs): 6.5, High work function (>5 eV), Thermal stability (>400°C).

ATO's high work function of 5.2 eV makes good contact with p-Si [50]. The absorption region lies at 3.65 eV for undoped tin oxide, and for FTO and ATO, it lies in the range 3.9 - 4.14 eV and 3.82 - 4.1 eV, respectively. This shift to a shorter wavelength region is an advantage for solar cell applications since it improves the short wavelength response of the cell [51]. Cadmium telluride and some amorphous-silicon solar cells can be grown on a SnO2 doped-covered glass substrate [50]. ATO layers improve the thermal stability of ITO in DSSCs and Cd-Te solar cells [52]. Also, increased electrical conductivity is observed on Sb doped SnO2 [53]. ATO proves to be a viable material because of its electrical conductivity, crystalline structure, visible light transparency, ultraviolet light absorption, and far and mid-infrared reflection capabilities. [54] [55] [56] Antimony tin oxide was bought and used from Sigma Aldrich (Figure 3). The particle size is less than 50 nm.

Figure 3: Antimony tin oxide from Sigma Aldrich

2.2. Cobalt Oxide

Cobalt II Oxide (CoO) is an electromagnetic material. The addition of paramagnetic metal oxides or ferromagnetic metal oxides like oxides of iron (Fe) and cobalt (Co) to oxides like tin oxide and chromium oxides. These materials are added to enhance the magnetic properties as well as infrared-reflectivity [57] [58]. Cobalt in various forms is used in solar cells. Cobalt oxide is used as a hole extracting layer in perovskite solar cells [59]. Cobalt doped nickel oxide has been explored as a hole transport layer [60] [61] [62] [63]. Copper-cobalt oxide shows high solar absorbance [64].

Adding cobalt to metal oxide improved the efficiency of solar cells [62]. Antimony Tin Oxide (ATO) with cobalt oxide increases its efficiency as an anti-reflective coating.

When CoO is added to ATO, it enhances the magnetic properties as well as enhance the infrared-reflectivity. [65]. CoO was bought from Alpha Aesar (Figure 4: Cobalt oxide (CoO) bought from Alpha Aesar).
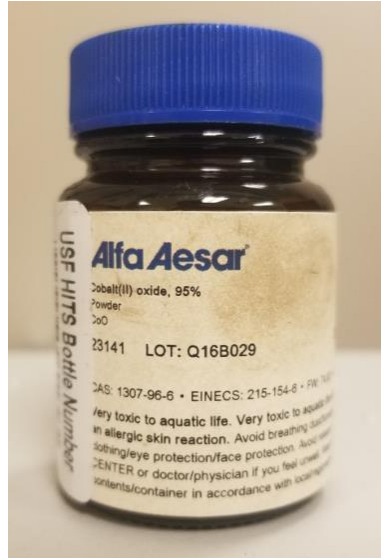
Figure 4: Cobalt oxide (CoO) bought from Alpha Aesar

2.3. Polystyrene

Polystyrene is derived from the monomer, styrene, and it is an aromatic hydrocarbon polymer. Polystyrene is an abundantly used polymer in the commercial world. Polystyrene has been used for varied applications, typically as a lightweight film in housing for packaging material and smoke detector alarms, disposable cutlery, and cast molds. This polymer is naturally transparent and can take the place of rigid plastic. Figure 1 is the structure of polystyrene.
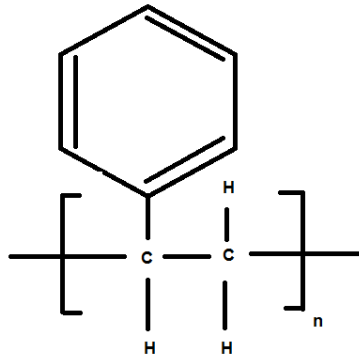
Figure 5: Chemical structure of polystyrene
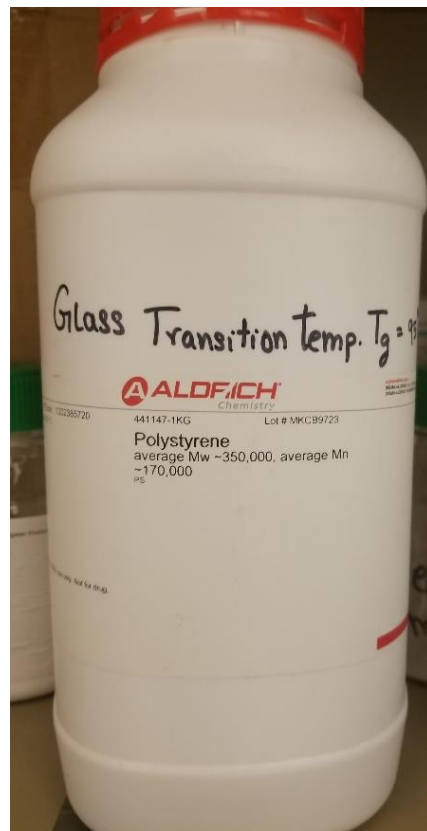
Figure 6: Polystyrene

As an abundant, transparent, and inexpensive resin, polystyrene offers favorable characteristics for use with the base materials of ATO and CoO to fabricate cost-effective thin films and structures. Polystyrene has good optical transparency as the polymer lacks crystallinity. Below the glass transition temperature of 93.8 C, the polymer can be molded easily without

affecting its chemical structure. 35000 molecular weight polystyrene was used for this study. The higher molecular weights enable better fiber formation during electrospinning.

2.4. Novel Elastic Polyimide

This super elastic polymer was obtained from Dr. Alejandro Rivera from Dr. Julie Harmon's lab at the University of South Florida's Chemistry department. The polymer was used as received. Figure 7 is the stoichiometric representation of the novel super elastic polyimide. Polyimides are known to have properties of high thermal stability, higher glass transition temperatures. They also have superior mechanical properties. The polyimide used has a molecular weight of approximately 44000 Da.

Glass transition temperature is the temperature above which the polymer or plastic looses its rigidity and becomes soft. The glass transition temperature is used to get a sense of the workable temperature range for the polymer.

Table 2: Stoichiometric formulation of flexible polyimide [66]

Sample	PMDA	TMMDA	D400 (LPPO)
XP0177 (PI-I)	0.50	0.10	0.40

Reprinted from "Formulation to Application: Thermomechanical Characterization of Flexible Polyimides and The Improvement of Their Properties Via Chain Interaction" by Alejandro Rivera Nicholls, 2019 retrieved: https://scholarcommons.usf.edu/etd/8679/

Schematic Representation of the Reaction Process

4,4'-methylenebis(2,6-
dimethylaniline)

10%

X= 6.1 Jeffamine D400

40%

Dissolved in GBL

50%

Pyromellitic
Dianhydride
(PMDA)

Dissolved in GBL
Reaction under N2 for 24H
Reaction temperature 80ºC

Polyamic Acid Precursor

Vaccum Distillation at 100ºC until all the solvent in extracted
Oven Cured at 200ºC for imide ring closure
Stored in the vaccum oven at 100ºC to dry the sample

Polyimide

Figure 7: Stoichiometry of the novel elastic polyimide [66]

Reprinted from "Formulation to Application: Thermomechanical Characterization of Flexible Polyimides and The Improvement of Their Properties Via Chain Interaction" by Alejandro Rivera Nicholls, 2019 retrieved: https://scholarcommons.usf.edu/etd/8679/

Based on the TGA results in Figure 8, the glass transition temperature T_g is found to be 328.6°C.

This is good for devices being used in room temperature environments.
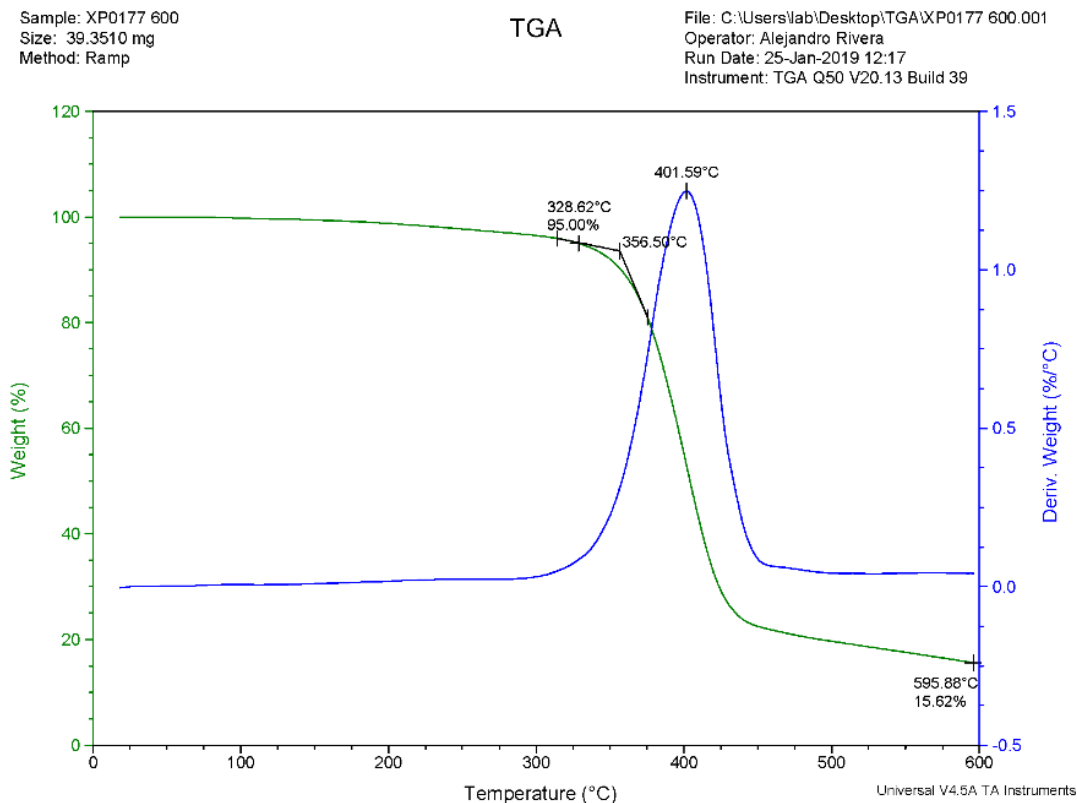
Figure 8: TGA analysis of XP0177 [66]

Reprinted from "Formulation to Application: Thermomechanical Characterization of Flexible Polyimides and The Improvement of Their Properties Via Chain Interaction" by Alejandro Rivera Nicholls, 2019 retrieved: https://scholarcommons.usf.edu/etd/8679/

2.5. Conclusion

A ferromagnetic oxide and metal oxide TCO composition, such as tin oxide, with antimony and cobalt oxide, can be used with polymers/polyimides to provide antireflecting fiber coatings properties for diverse applications. When fabricated as nanostructures, particularly nanofiber membranes, this material composite of CoO-ATO can be used as anti-reflective coatings. Also, as

19

a nanofiber membrane, the large surface area and the ability to control deposition are advantageous.

Chapter 3: Fabrication of Nanofiber Membranes

Polymer nanofibers have been of interest for the past decade. The large surface area to volume ratio enhances the chemical and mechanical properties of materials. Different processing methods are used to achieve different morphology and physical properties of the materials. Inthis study, an electrospinning process was used to make the fiber membranes. The drawing of a polymer from its polymeric solution into nanofibers by applying an electric field is called electrospinning. Electrospinning is a simple, efficient, low-cost fabrication method. [67]

3.1. Electrospinning Setup

The experimental setup Figure 9, An electrospinning system is pictured. The assembly has a step-up voltage supply, a syringe pump apparatus, and a collector plate. Harvard apparatus programmable syringe pump was used. A base, for example, an aluminum foil is wrapped on the plate is used. Aluminum foil is chosen because it is pliable and can be conformed over any collector substrate. Its availability and high electrical conductivity make it a good choice as a collector substrate.

Electrospinning requires high voltages to create strong electric fields between and around the needle and the collector plate. The voltage regulator used operates from 1kV to 30 kV. The positive of the AC electrode is connected to the syringe. The neutral electrode is the ground and connected to the collector plate, forming an electric field between the needle and the collector plate. When the solution in the needle is pumped out, the solution is charged up by the high voltage supply. This charged solution ejecting out of the syringe pump pursues an electrical ground. Thereby it is collected on the foil. As the polymer solution ejects from the needle, if there is no

electric field applied, it accumulates into a bead due to the lack of overcoming the surface tension of the polymeric solution. However, in the presence of a high voltage electric field, this sphere is drawn out of the needle into a cone, and fibers are formed. This is a hydrodynamic process and is called the Taylor cone. A thin fiber is formed from the tip of the cone. The path traced by the nanofiber as it moves from the needle to the collector plate is the path of the electric field.

The polymeric solution is mixed in a beaker or a glass vial so that the solvent used for polymers does not dissolve a polymeric container. A magnetic stirrer of appropriate size is used to keep the entire volume of the solution continuously agitated. A parafilm is used to seal the beaker. A vial with Teflon lined cap is used prevent solvent evaporation. The gap between the cap and the vial is sealed with parafilm for additional protection.

The syringe pump is a programmable infusion device. The desired infusion rate can be set. The infusion rate is the volume of solution ejected out per unit time. This infusion rate can be set if we know the diameter of the syringe cylinder. It was measured using a caliper. This data point was entered into the syringe pump system. The syringe is filled with a homogenous polymer solution. It is loaded on the pump and is programmed for a specific infusion rate. The infusion rate must be set such that all the solution that is ejected out can be attracted onto the collector plate and is electrospun. The voltage supply is turned ON. In this way, the polymer's solvent evaporates, and the polymer is left behind on the foil as nanofibers. The distance between the needle tip and collector plate should be at an optimum level so that the electric field between the collector and the needle is strong enough to spin fibers, and it should be far enough to let the solvent evaporate off from the solution so that as the fibers are formed. In case the collector plate is too close to the syringe, the wet or solvent-laden fibers collect one on top of the other and deposit it as a thin film.

Membranes required to be peeled off the collector plate are simpler to peel when spun onto a release paper. Release paper is affixed on the collector plate using tape.
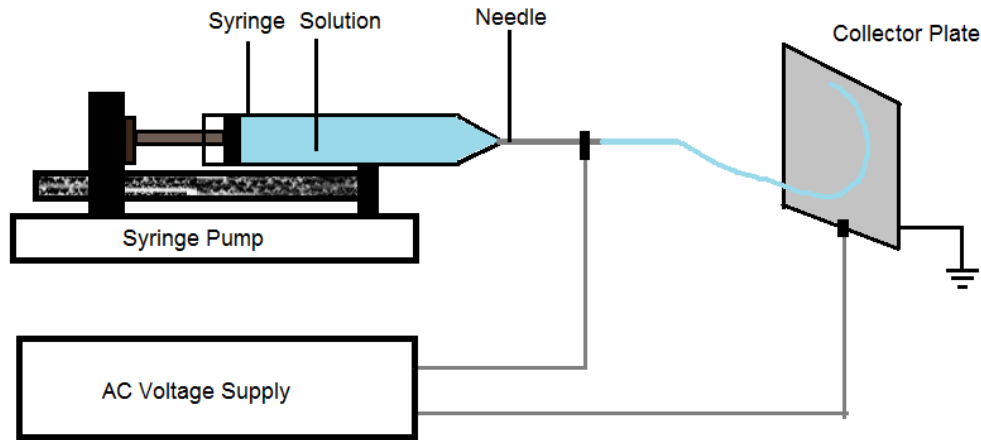
Figure 9: Electrospinning setup

3.2. Conclusion

The experimental conditions that affect the fiber formation, fiber morphology are described.

3.2.1. Parameters Influencing the Electrospinning Process

The electrospinning process is very sensitive to all parameters that can vary. The parameters that influence electrospinning proves are as follows,

- *Solvent:* A fast evaporating and preferably electrically conducting solvent produces fibers more readily.

- *Polymer molecular weight:* Polymer molecular weight is related to viscosity. Higher the molecular weight, higher the viscosity. More viscous polymers form fibers readily. Use of polymers with long molecular chains or bigger molecular weights are recommended. Also, if the viscosity is too high, it is difficult to pump the solution out of the syringe in a consistent flow.

23

- *Voltage:* Voltage is applied at the needle and the collector plate is grounded. This creates an electric field between them. The polymeric solution at the needle tip is whipped into fibers. If observed closely, the fibers seem to follow the path of electric field.

- *Current:* since there is no physical contact between the needle tip and collector plate, and because of the disctance between them, roughly 15 to 20 cms, the current is extremely low.

- *Distance from needle tip to collector plate:* The collector plate should be at a distance such that, when the fiber is spun onto it, the solvent evaporates. If placed too near, the fibers are still wet with solvent.

- *Infusion Rate:* Infusion rate is the rate at which the polymeric solution is fed into the needle. Continuous fiber formation is preferred, to enable this, there needs to be a steady infusion of polymeric solution. If the infusion rate is set too high, the solution drips down without forming fibers, wasting valuable material.

3.2.2. Parameters for Spinning the CoO ATO Fibers

The following are the parameters used for electrospinning CoO ATO fibers.

Table 3: Parameters for optimum electrospinning CoO ATO fibers

Parameters	CoO ATO fibers for Solar cells	CoO ATOfibers for infrared sheath
Voltage applied	15 kV	20 kV
Current noted between the needle and collector	1 μA	1 μA
Infusion Rate in ml/hr	2	3
Distance from Needle Tip to collector plate in cm	15 cm	10 cm
Stir Time	1 day	1 day

Chapter 4: CoO-ATO Nanofiber ARC Membranes for Solar Cells

Thirty six percent of light incident on a polished silicon wafer surface is wasted by reflection [68]. Lowering silicons top surface reflectivity by texturing is one of the most standard methods for improving Si solar cells' conversion efficiency.

In this work, it is noted that the refractive index of silicon is 3.5, and the refractive index of air is 1. An ARC with a refractive index between 1 and 3.5 should be chosen. By developing a surface texture on a Si substrate, the following three effects can be observed:

- surface reflection is reduced

- Increase in light absorption as the optical path length increases by diffraction

- Internal reflection that reduces the amount of escaping light is enhanced.

- Adding a fiber membrane with the same characteristics of an optical anti-reflective layer. This system does not utilize an expensive setup for deposition and etching and thereby is a quicker and lower cost of production.

CoO-ATO nanofiber anti reflective fiber membranes can offer a textured surface for solar cells and lead to the benefits discussed above. The characterization of these nano textured surfaces will demonstrate the suitable properties for enhancing solar cell performance. This chapter investigates the thermogravimetric analysis (TGA) of the CoO ATO fibers for solar cells, refractive index of the ARC. Testing has been performed under sunlight as well as under standard AM 1.0 conditions.

4.1. Thermogravimetric Analysis

Thermogravimetric analysis is a valuable tool that helps in understanding the thermal stability of the material. It is an analytical technique used to determine thermal stability and identifying its fraction of volatile components. This is done by observing the weight change that happens as the sample is heated at a constant rate. There are three types of TGA: Dynamic TGA, Static TGA and Quasistatic TGA.

- Dynamic TGA: the temperature increases as the mass is recorded. It helps in recording the degassing and the temperature at which degassing occurs.

- Static TGA: Temperature is held constant as the mass is measured. This method is used to obtain more information on the change of material at a specific temperature and study its ability to withstand a given temperature.

- Quasistatic TGA: In this method, the temperature is ramped up and held at different temperatures for a specific period while ramping up. This way, the disintegrating or decomposition of materials at different temperatures are studied.
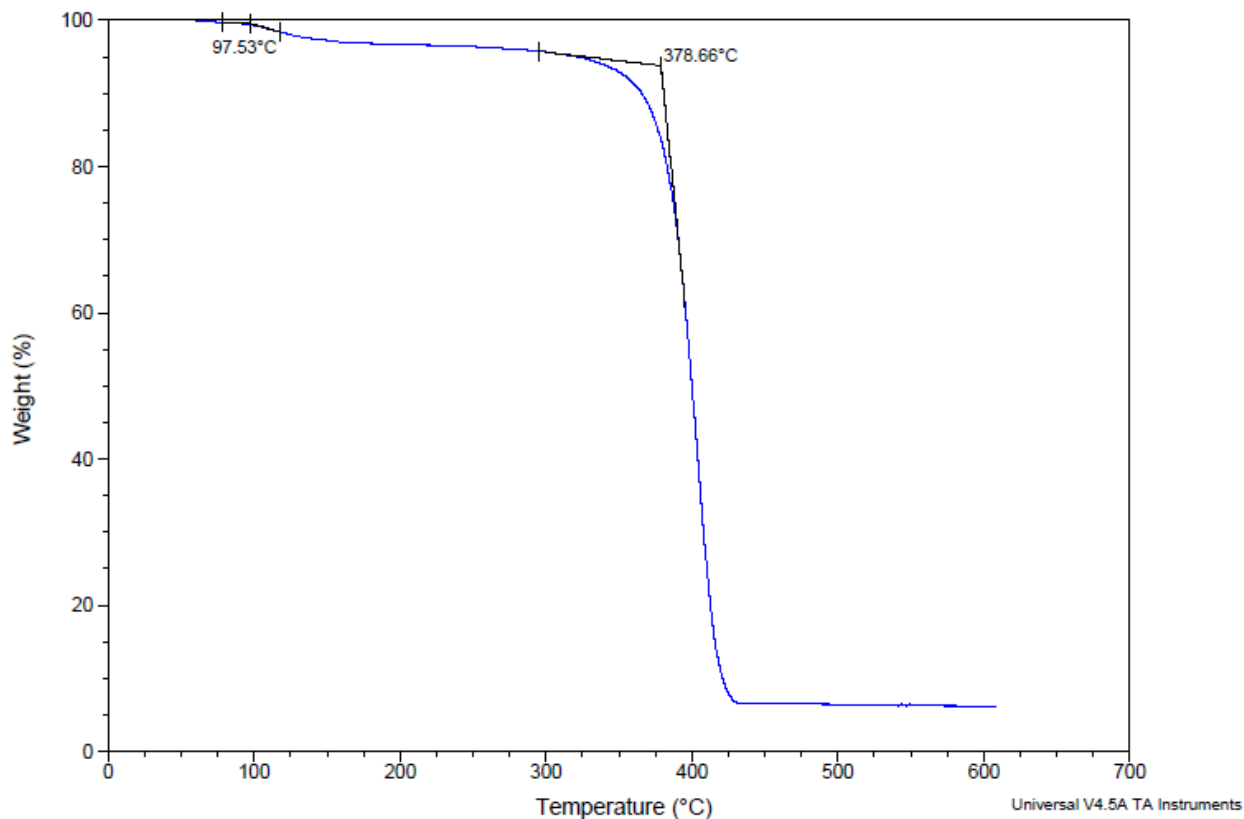
Figure 10: Dynamic TGA analysis of ATO CoO PS fibers

Glass transition temperature and decomposition temperature of the polymeric composite. The results from TGA can be interpreted to understand the workable temperature of the polymer. TGA analysis was performed on the ATO CoO membrane to find the degradation temperature of the composite membrane.

A sample of weight between 16 to 20 mg was placed on a tared 100 mL platinum pan. This pan is then placed in a TA TGA analyzer's standard furnace. The heating took place in a nitrogen atmosphere at room temperature. Samples are heated to 600°C with a ramp rate of 10°C/min. Figure 10 shows the TGA analysis result of the CoO ATO ARC membrane.

Glass transition temperature was found to be 97.53°C and disintegration temperature was found to be 378.66°C. If the polymer was heated gradually from room temperature, initial disintegration starts at 97.53°C and completely disintegrates at 378.66°C. If the polymer composite is to be incorporated in a fabrication process, the workable temperature while retaining all its physical and chemical properties is up to the glass transition temperature.

4.2. Refractive Index

The refractive index for CoO ATO ARC on silicon wafers has been measured and studied. The refractive index and the corresponding extinction coefficient are optical properties or characteristics of thin-film materials. When light passes through a medium, some of the light is attenuated. This attenuation coefficient is included in the complex refractive index.

$$n^* = n + ik$$

where n is the refractive index, n^* is the complex refractive index and k is the attenuation constant. Crystalline materials usually have only the real part of the refractive index. Ie, there is no imaginary k value associated with it. However, in the case of amorphous materials, there is an attenuation constant (k) associated with the refractive index. Samples used to measure refractive index are made by spin coating the CoO ATO ARC solution on silicon wafers. The wafer is RCA cleaned. Next, for spin coating, the entire surface of the wafer is covered with a CoO-ATO solution. A speed of 1500 RPM is chosen, and the duration is set to 45 seconds. A slower RPM on the spin coater results in a thicker film. After the film dries, it is peeled off from the wafer. Peeled thin film is used for measuring the refractive index. The stand-alone thin film is considered as a substrate for ellipsometer measurements.

Rudolph ellipsometer was used to measure the refractive index of the composite. This ellipsometer has a laser light source with a wavelength of 632 nm. The refractive index was found

to be 1.424, with an extinction coefficient of 0.045. These are the n_s and k_s values, respectively. Here the subscript s refers to a substrate. This is in accordance with previous results [69].

4.3. Modified Solar Cell Structure with CoO ATO Nanofiber ARC

Crystalline solar cells manufactured by Q-cells have been used in this study. The top layer of the as-bought solar cell is a Silicon Nitride (Si_3N_4) layer. Silicon nitride is the anti-reflective coating layer. The surface morphology of the Si_3N_4 ARC was investigated by scanning electron microscopy (SEC). Figure 11 shows an SEM image of the top layer of the as bought solar cell. Figure 11 is the initial silicon nitride ARC before etching. Pyramid facets on the structure surface is noted. The thickness of this layer was approximately 1 micron to 700 nm as measured by ellipsometry.
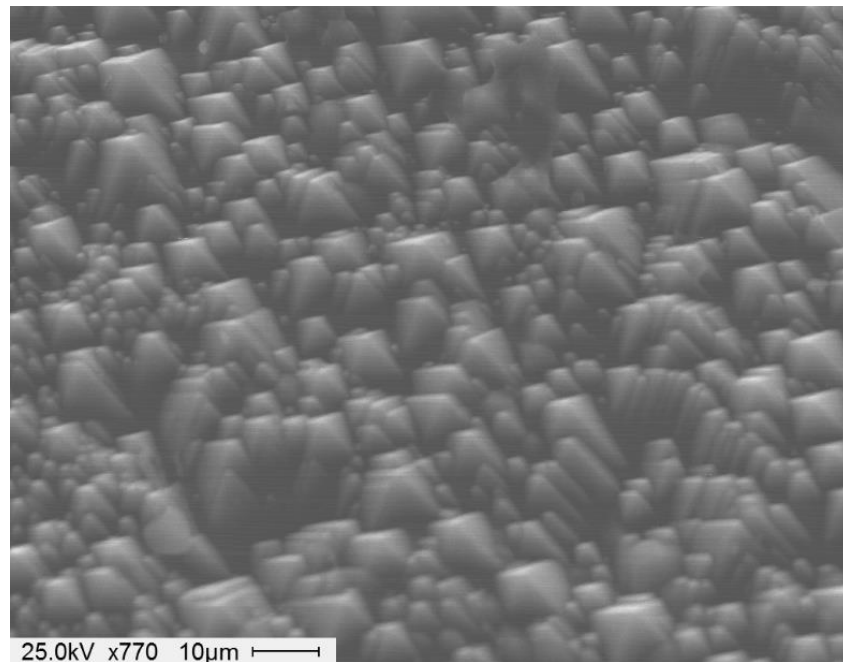

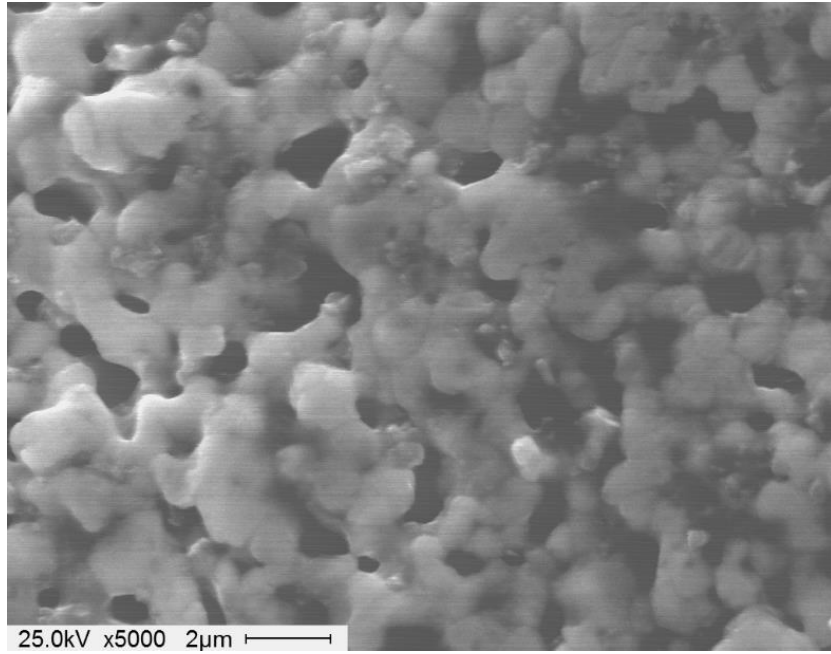Figure 11: Image (SEM) of SiN ARC layer before etching showing a pyramid structure

Figure 12: Image (SEM) of the silver bus bar on top of the solar cell before etching.
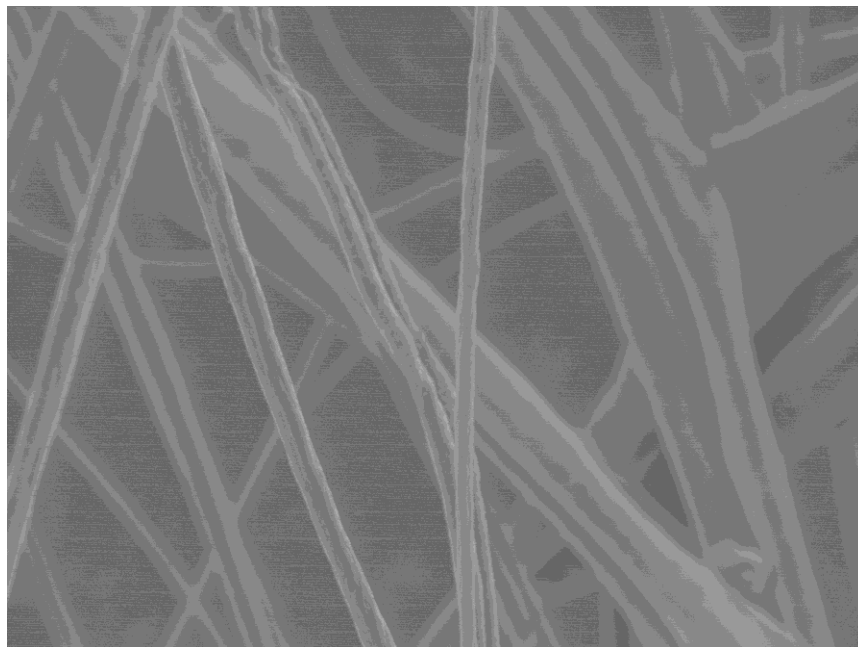

Figure 13: Image (SEM) of a freestanding CoO ATO mesh

The surface morphology of the SiN ARC reveals pyramids randomly distributed across the unetched surface and a flattening of the pyramid facets on the etched surface. In anti-reflecting coating (ARC) technology, the efficiency of anti-reflective coatings is improved by choosing an appropriate material and also by introducing structures in surface morphology. Pyramids, cones, cubes, hexagons, rods etc., have been explored [13] [14].

DRIE etching (Deep Reactive Ion Etching) is a standard tool in the fabrication of MEMS and semiconductor devices. This method is a very anisotropic etch mechanism. A DRIE etch performed when etching is required with high precision. Deep trenches and wells can be etched on the surface of crystalline silicon, which is very important while fabricating MEMS sensors. Many MEMS structures have narrow and deep trenches that facilitate sensing. Usually, while fabricating these trenches with wet methods, the trenches collapse. During the drying or liquid extraction, there is a high chance of narrow aspect ratio materials getting damaged and fail due to capillary action. The etch rate for silicon dioxide and silicon nitride in the DRIE mechanism is the same. Etch rate of the top silicon nitride layer in less than a minute.

The DRIE method is a combination of physical as well as chemical etching. Since DRIE etching etches chemically and by ions bombarding the surface, the chance of a device failure is lower. RF power of 4200W power was used at the top and 400W of power at the bottom to provide a field for ions to travel and perform the etch process. Sulfur hexafluoride SF_6 is used to etch silicon-based layers like silicon dioxide ($SiO_{2)}$ and silicon nitride (Si3N4). Silicon wafers were scribed into rectangles so that the longest dimension is less than 4 inches. This way, it would fit the sample holder on a DRIE etch system. Samples were etched for 30 seconds. Oil is used to hold the samples in place. Figure 15 shows the samples after the DRIE etch. After the etch, to remove this oil, cells are heated up in oxygen plasma in Plasmaline 415, as shown in Figure 16: Plasmaline

415 for removing organic compounds after DRIE etch. Oxygen plasma then burns off the oil without affecting the cell.
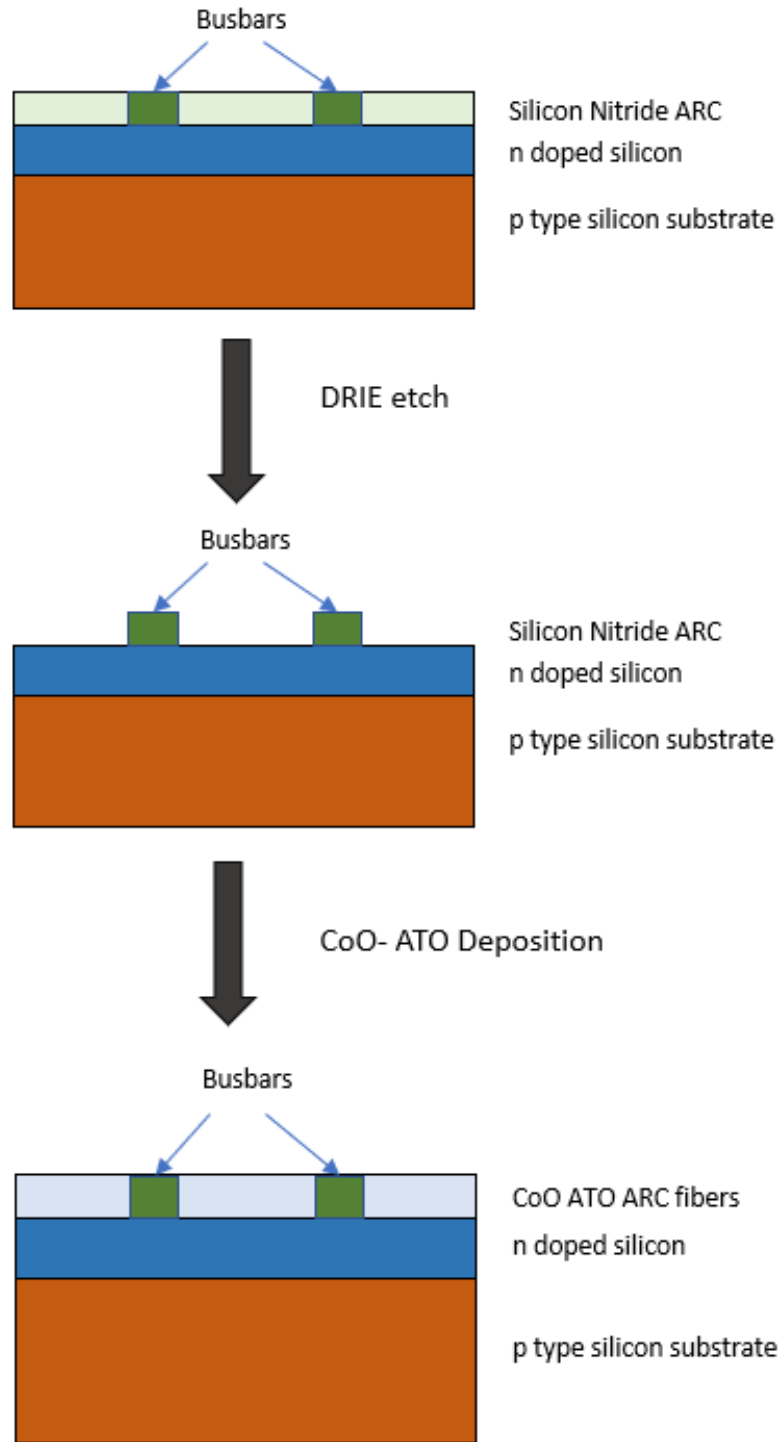
Figure 14: Schematic diagram of CoO-ATO deposition on solar cell

Figure 15: Solar cell after DRIE etch

Figure 16: Plasmaline 415 for removing organic compounds after DRIE etch

A solution of CoO – ATO in polystyrene is prepared to make fibers. The composition is as follows: 0.1 percent cobalt oxide, 2 percent ATO powder from sigma Aldrich, 12 percent medium molecular weight polystyrene, and 85.9 percent chloroform. These are weight-to-weight ratios. A 3 mL syringe is loaded with the solution and Electrospun onto aluminum foil.

For CoO ATO thin film samples, DRIE etched solar cells were spin-coated with CoO ATO Solution. For spin coating, the chamber was lined with aluminum foil, and the solar cell was placed

on the chuck. The speed was ramped to 500 rpm for 5 seconds and to 3000 rpm for 60 seconds. When the spin coating is completed, the cells were set to dry for 2 hours before testing them.

For the fiber ARC samples, fibers of CoO ATO have been spun on top of the DRIE etched solar cell. The solar cell was stuck at the end of a wooden spatula by Kapton tape. The spatula was held by hand. When the system is turned ON, there are a few inconsistencies in fiber formation, like electrospraying or solution accumulation, for a few seconds. Once a consistent fiber formation is noticed, the DRIE etched cell is exposed to the fibers for 30 to 45 seconds. This method was adopted to avoid the inconsistent fibers getting on the cell. Figure 19 shows the EDS result before the solar cell was etched. Figure 20 is the EDS result after the cell is DRIE etched and coated. An absence of the nitrogen peak but a presence of carbon peak is noticed. This shows that the SiN ARC is completely etched down. The presence of carbon indicates the CoO ATO ARC peak.
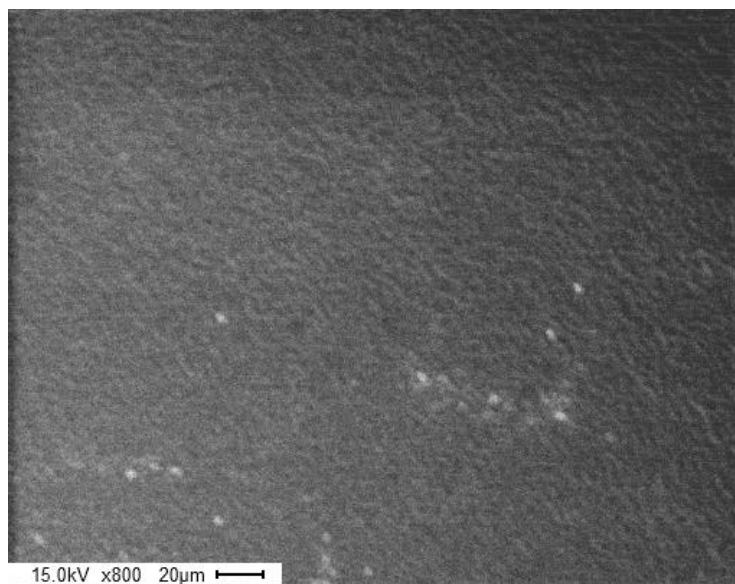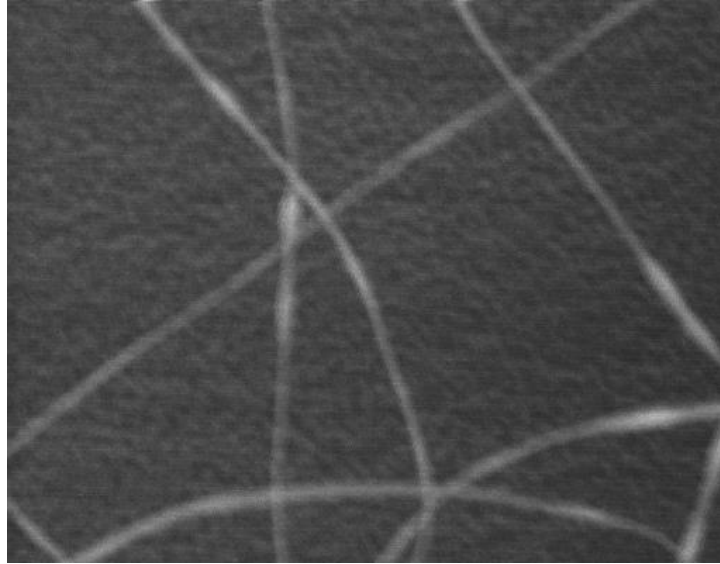

Figure 17: SEM after DRIE etch

Figure 18: Etched solar cells coated with CoO ATO
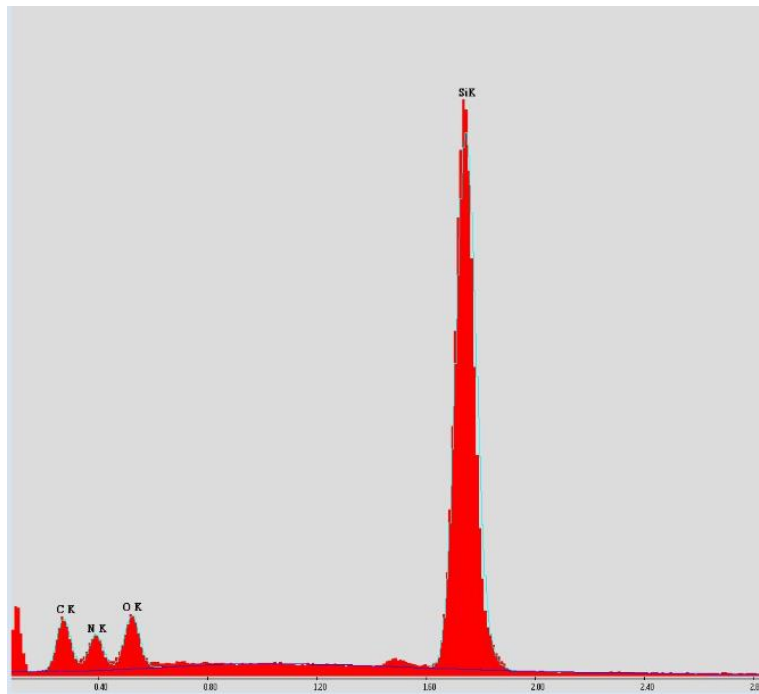
Figure 19: EDS of the solar cell before DRIE etching
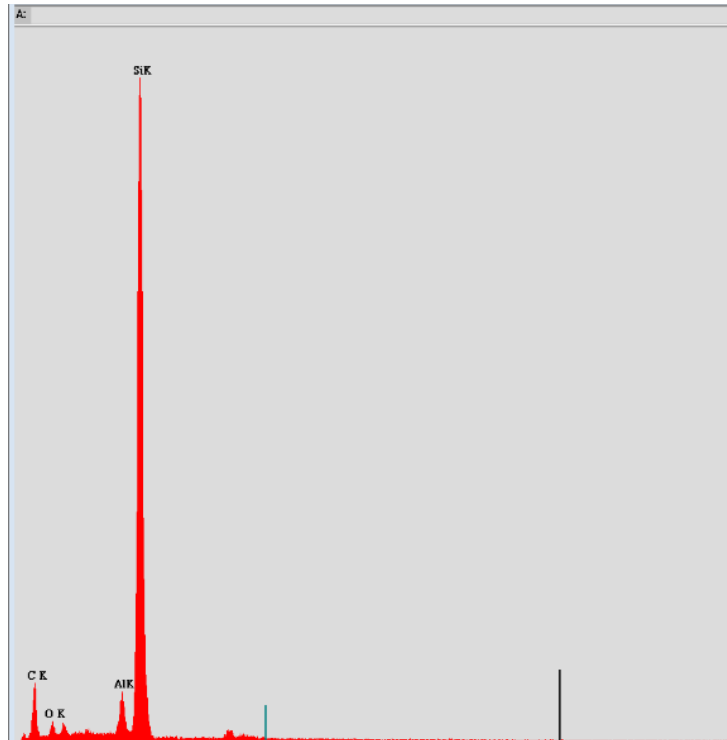
Figure 20: EDS of the solar cell after DRIE etch and fiber deposition

4.4. Testing Performed Under AM1.0 G Solar Radiation.

A series of tests were performed under standard AM 1.0 radiation. Readings were recorded and graphed, as shown in Figure 21, Figure 22, Figure 23 and Figure 24. These are plots of current density vs. voltage. In the reverse-biased region, electrons go from anode to cathode, and hardly any current is noticed. In the forward bias, electrons go from anode to cathode. Initially, an injection barrier is seen. After overcoming the injection barrier, the current starts flowing. These graphs are plotted under illumination. It should be noted that under illumination, photocurrent can occur without an external voltage.

In the graph, the current density J value when the applied voltage V =0 is J_{SC}. This is the short circuit current density. The value of V when J=0 is the V_{OC} of the solar cell. From Voc, we can obtain the fill factor by using the equation

$$FF = \frac{V_{MP}I_{MP}}{V_{OC}I_{SC}}$$

The fill factor has been determined using the above equation.

Figure 21 is a plot of current density against voltage applied across a solar cell with no anti-reflecting coatings. Five samples have been studied. In this plot, the average value of the current density of the solar cell is observed to be 18.33 mA/cm^2.
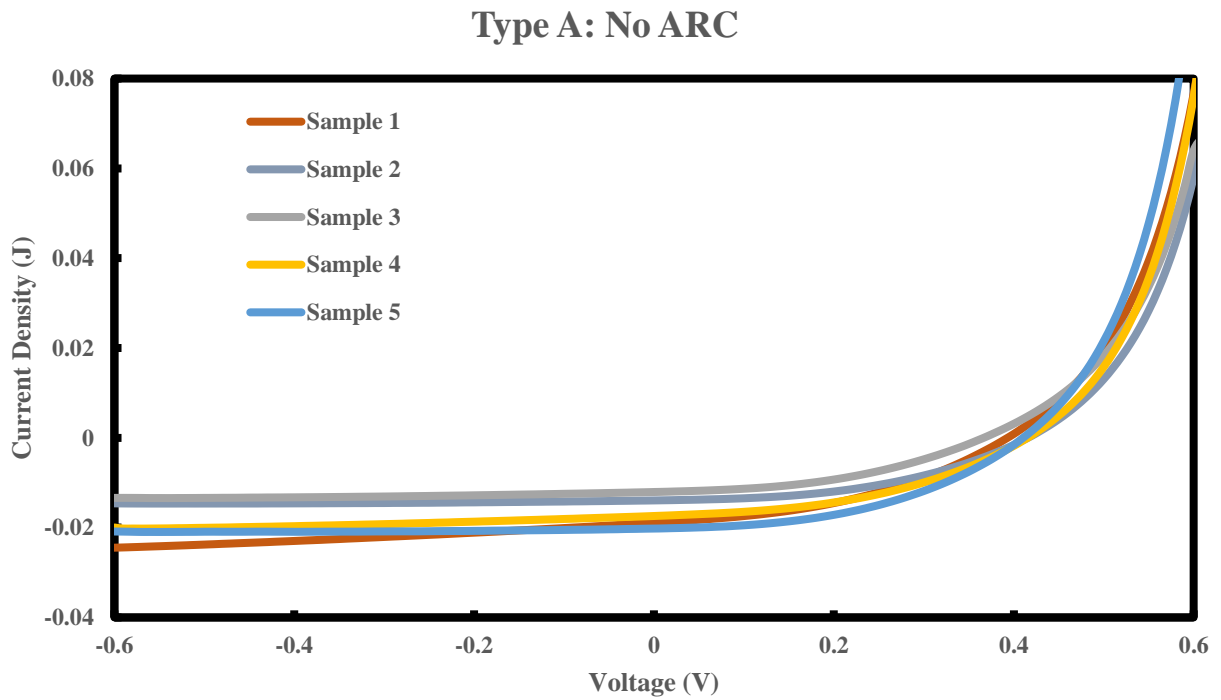
Figure 21: Type A: No ARC layer
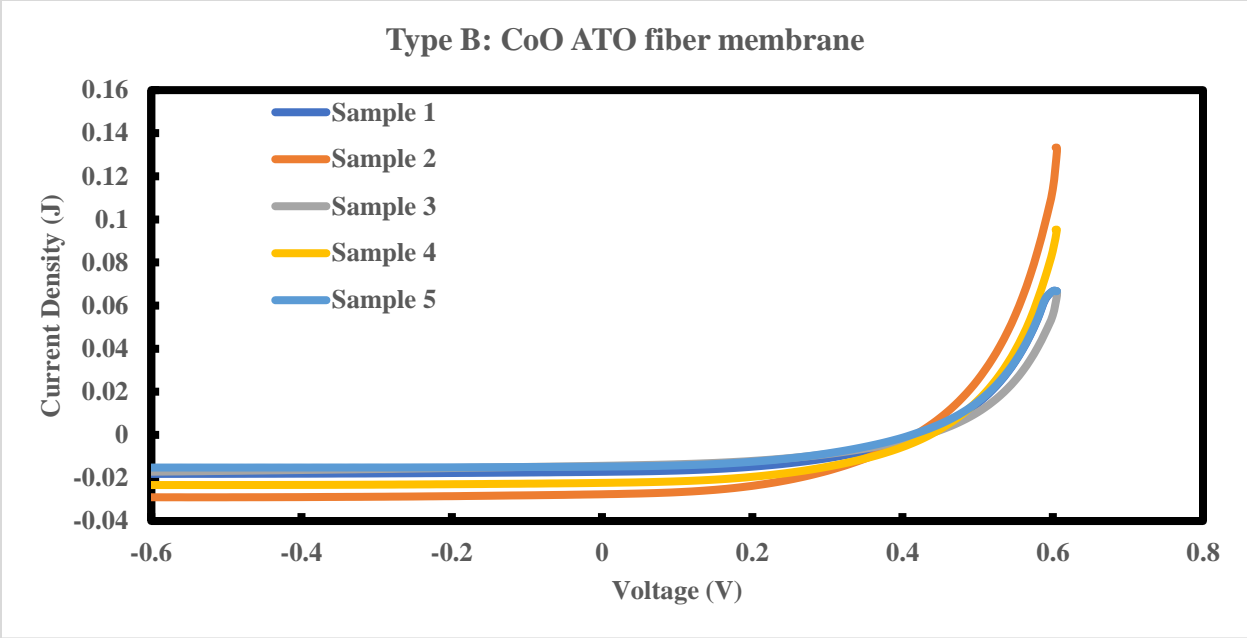
Figure 22: Type B Solar cell with CoOATO ARC layer
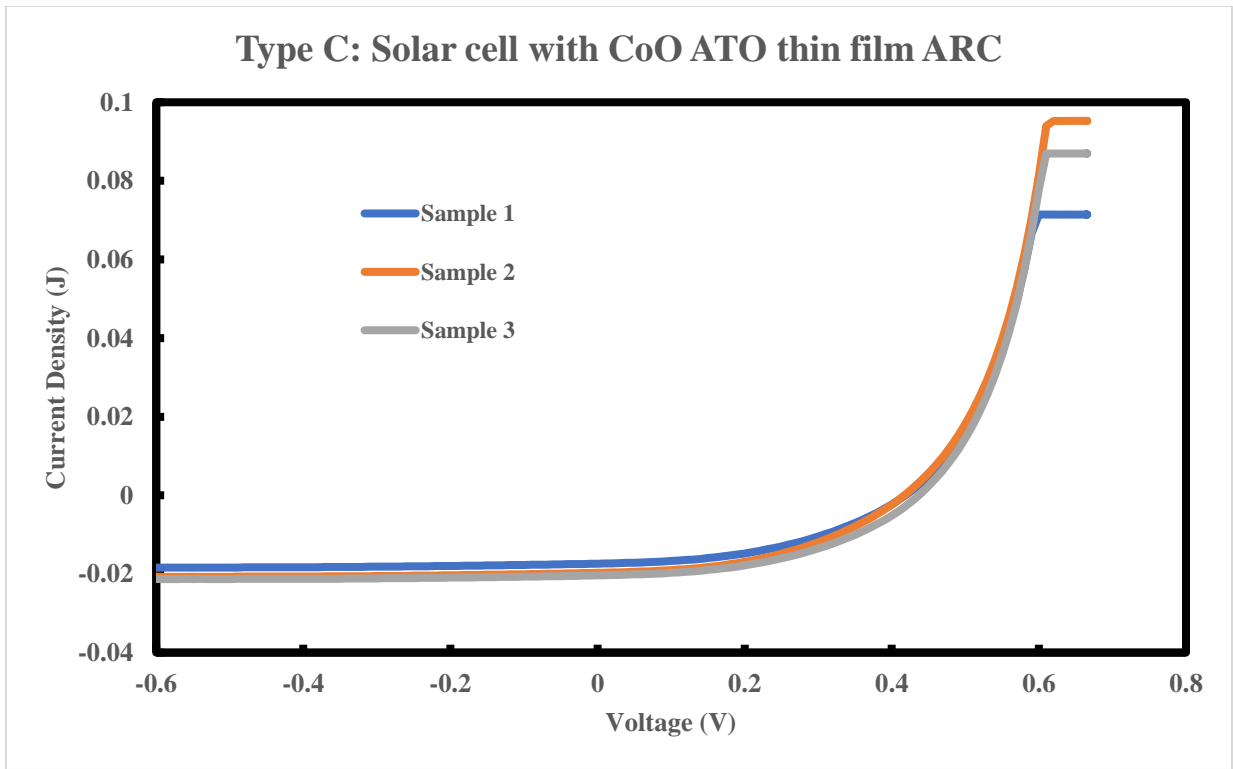
Figure 23: Type C: Solar cell with a thin film coating
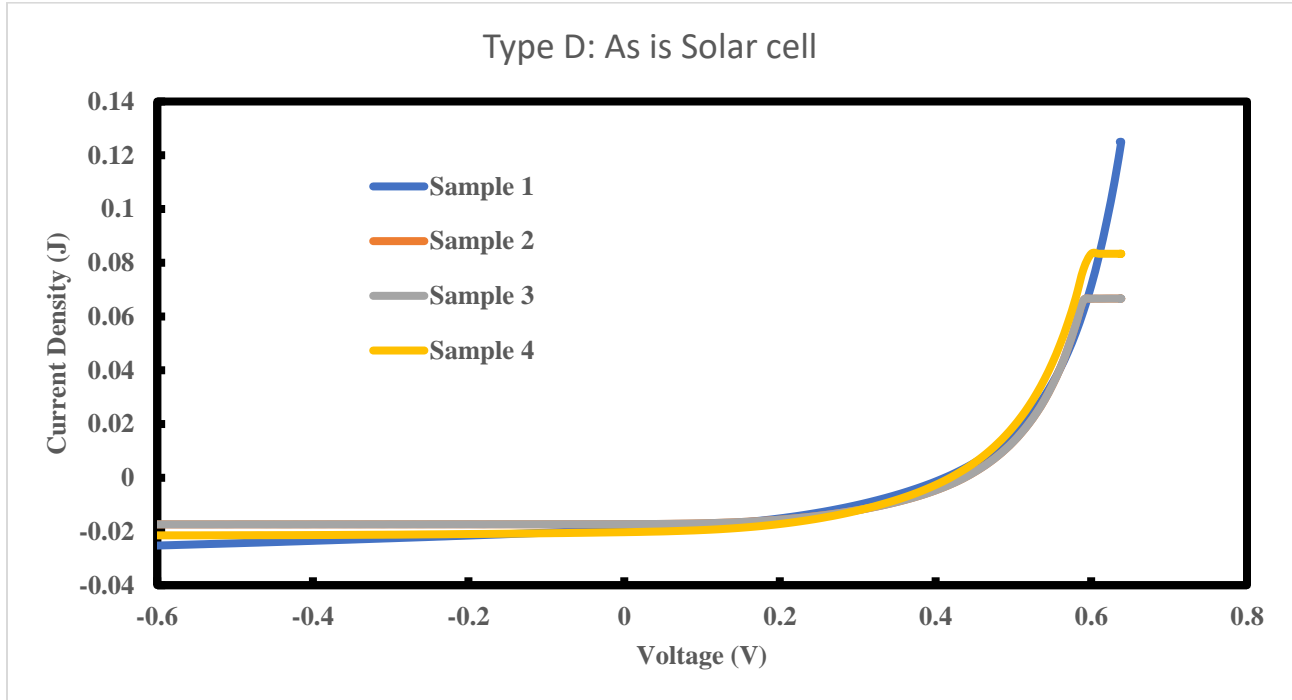
Figure 24: Type D: As is solar cell

Table 4: Solar cell current density measurements at AM 1.0

Sample Name	Description of Samples	Average Current	Average Current Density J_{SC} (mA/ cm^2)	Average Open circuit voltage V_{OC} (mV)	Fill Factor	Efficiency η %
Type A	Solar cell with no ARC Layer	18.33	16.53	396	.869221	5.6
Type B	Solar cell with CoO ATO fiber ARC	22.2	19.23	430	.876190	7.24
Type C	Solar cell with CoO ATO thin film ARC	19.5	18.73	423.3	.874580	6.94
Type D	As is solar cell	19.12	19.12	422.5	.873959	7.06

4.5. Testing and Results of CoO-ATO Nanofiber ARC under sunlight

A series of tests were performed under sunlight on July 23 and 24, 2020 under partially cloudy weather. Readings were recorded when the sun was piercing through the clouds. Figure 25 is an image of a DRIE etched sample tested for the short circuit current under sunlight. Figure 26 is an image of a DRIE etched solar cell with CoO ATO ARC tested for short circuit current under sunlight. Figure 27 is an image captured while testing the solar cell with a SiN ARC for short circuit current under sunlight.

Figure 25: Solar cell scribed into 6cm X 4cm, DRIE etched. No anti-reflective coating.

Figure 26: Solar cell scribed into 3.5 X 2.5 cm, and DRIE etched Coated with CoO ATO

Figure 27: As received sample scribed into 3.5 X 3.5 cm

Table 5: Solar cell current density measurements under sunlight

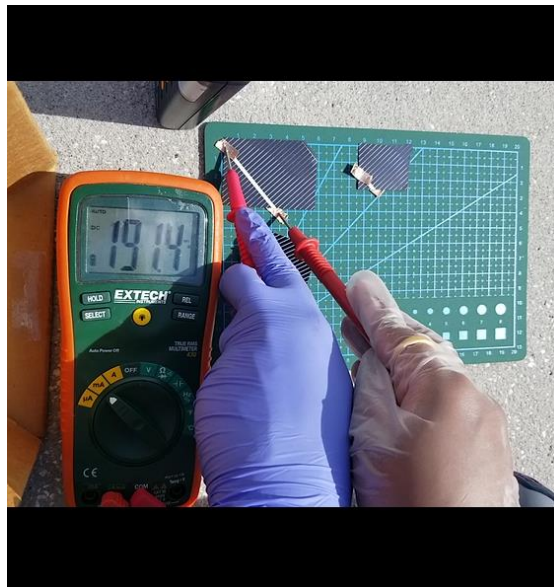| Sample Name	Sample Description	Dimensions	Area (cm^2)	Max Current reading (mA)	Current Density (mA/cm^2)
Type A	No ARC Layer	6cm X 4cm	24	191.4	7.968
Type B	As bought solar cell (SiN ARC)	3.5cm X 3.5cm	12.25	105.3	8.59
Type C	Solar cell with CoO ATO ARC	3.5cm X 2.5cm	8.75cm^2	93.8	**10.72**

It should be noted that testing under sunlight conditions was challenging due to lack of optimum position of the sun. Therefore, both measurements for solar cell current density measurements under AM 1.0 and sunlight were investigated.

4.6. Conclusion

This chapter explored CoO ATO fibers as an antireflecting fiber coating (ARC) of a solar cell. Standardized AM 1.0 measurements were made. The current density versus voltage measurements was made under illuminated conditions. The resulting plot gives us the current density versus voltage measurements. From the graph, it is to be noted that V_{OC} is measured as the value of voltage when the current density is 0. The short circuit current density is the current density value when V_{OC} is 0.

The spin-coated samples had Voc of 423.3 mV. The fiber coated sample Voc was noted as 430 mV. The maximum open-circuit voltage was noted in CoO ATO fiber samples. The graphs obtained indicated a 2% increase in V_{OC}. Respective fill factors were determined.

The solar cells coated with fibers were measured in standard AM 1.0 radiation conditions as well as outdoors. Under the standard conditions: 1. The efficiency improves 29% from a no ARC solar cell to a CoO-ATO nanofiber ARC. 2. The efficiency improvement of 3% is seen comparing the as-is solar cell versus the nanofiber ARC solar cell. Under sunlight, 34% increase in current density is noted from the bare cell to cell with CoO ATO ARC solar cell. A 20% increase in

current density is noted from as bought solar cell to CoO ATO ARC solar cell. In both cases, improved efficiency is noted.

Chapter 5: Super-elastic CoO-ATO Nanofiber Membrane as a Thermal Sheath

A novel super-elastic polymer made of Pyromellitic dianhydride (PMDA), Jeffamine D400 and 4,4'-Methylenebis (2,6-dimethylaniline) (MBDMA). The solvents used in the synthesis were a mix of THF and DCM. The synthesized polyimide was used as received from Dr. Harmon's lab at USF. High elasticity was noted in the thin film structure, and when electrospun, the elasticity improved. This led to the idea of fabricating a super elastic infrared reflecting membrane.

5.1. Fabrication

The super-elastic membranes were electrospun using the electrospinning setup described in chapter 3. The polyimide (XP0177) solution was prepared as follows. The synthesized polymer (XP0177) is mixed into DCM (Dichloro Methane). This mixture is agitated in a vortexer for half a minute and sonicated or stirred on a magnetic stirring plate until the polymer dissolves. It is observed that 12 grams of the polymer mixed in with 40 grams of DCM produce the most elastic fibers. To the polyimide solution, two percent of ATO and 0.1 percent of CoO were added and mixed for 2 hours and electrospun. A 3 mL Luer lock syringe was loaded with solution. A 27-gauge needle was used to spin fibers. A fixed voltage of 20 kV was applied between the needle and the collector plate with an infusion rate of 3 mL/hour collection distance was set to 20 cm. The membrane was folded twice and used for the infrared test. The thickness of the membrane collected on the collector plate is 0.3 mm.

From the SEM image, as shown in Figure 28, it is clear that the electrospinning method produces fibers that interlace randomly. For the tensile testing, the following five samples were used 1) XP0177 as a thin film, 2) XP0177 electrospun fibers collected in random orientation, 3)

XP0177 fibers electrospun fibers collected in perpendicular orientation, 4) XP0177 fibers collected in a parallel orientation, and 5) XP0177- CoO ATO composite fibers collected in random orientation. SEM imaging and AFM measurements were performed to characterize the fiber membrane. Tensile testing was done to analyze the elasticity of the electrospun fiber membrane.
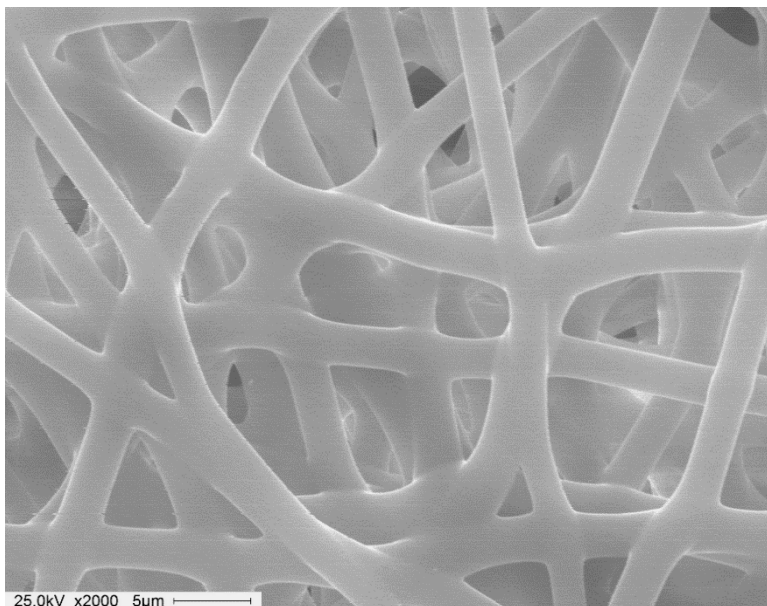
Figure 28: CoO ATO XP0177 Super Elastic fiber membrane

5.2. AFM

Atomic Force Microscopy (AFM) was performed on the CoO ATO XP0177 elastic membrane to study the surface roughness. When CoO ATO XP0177 membrane is electrospun, and the new fibers deposit on the already existing fibers. When this happens, the overlap area merges and form knuckle like structures. XP0177 has a smooth surface since all the fibers formed are held down by the already existing fibers. This way, the membrane is very uniform and with minimal roughness in the order of 117.9 nm. A sample of 50 micrometers X 50 micrometers was analyzed. The maximum height traversed by the AFM tip is 561.12 nm. Figure 29 and Figure 30

are images from atomic force microscopy analysis of the membrane. Figure 29 is the 3D view of

a 50 micrometer X 50-micrometer scan area.
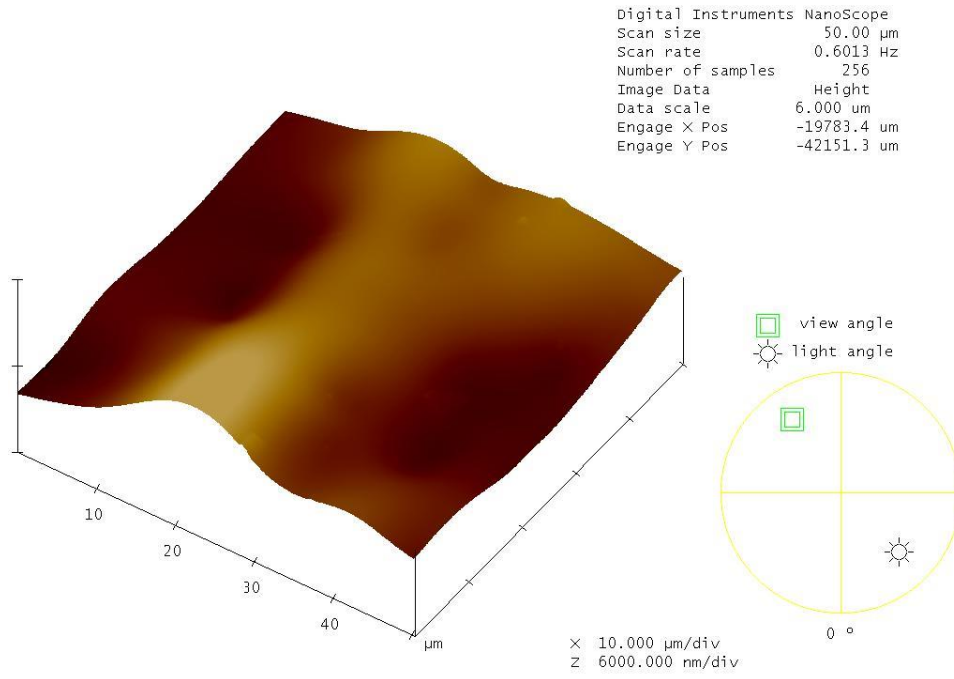
Figure 29: AFM surface roughness measurement

Figure 30: AFM surface roughness analysis

5.3. Tensile Testing

Tensile testing is a material characterization that studies the materials' response to stress. Tensile strength characterization of the fiber membrane was done using Shimadzu AGS-J tensile tester to measure the displacement of samples. A 50 N load cell was used. The tensile tests were done at a crosshead speed of 25 mm/min at room temperature according to ASTM D638. Dog bone cut samples from fiber membrane samples had thicknesses ranging from 0.16 to 0.20 mm, as shown in Figure 31.
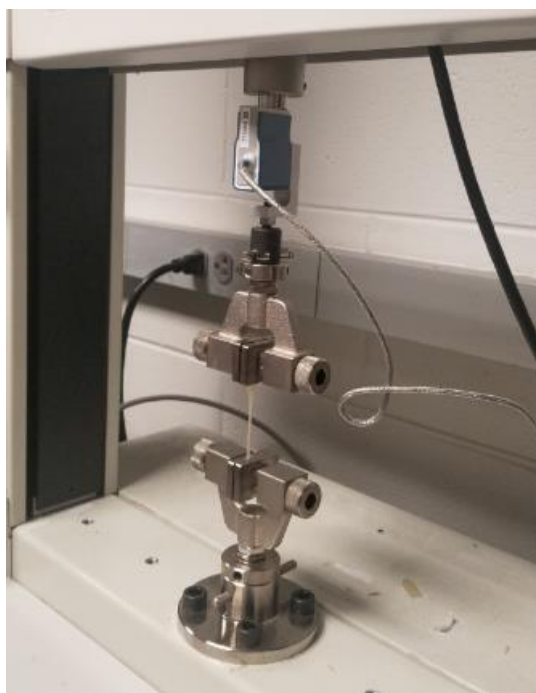
Figure 31: Tensile testing setup

5.4. Infrared Camera Test

A FLIR brand infrared camera was used to analyze the infrared properties of the electrospun membrane on a heat source. An infrared camera has a detector or lens which absorbs infrared light and converts this infrared light to electrical signals and images of the area.

The heat source used for the experiment was a hot plate. The hot plate was turned on and set to the minimum temperature setting. As shown in Figure 33, the hot plate temperature was

noted to be 39.7C. Figure 35is a composite picture consisting of the image from an infrared camera on the top and a regular image on the bottom.
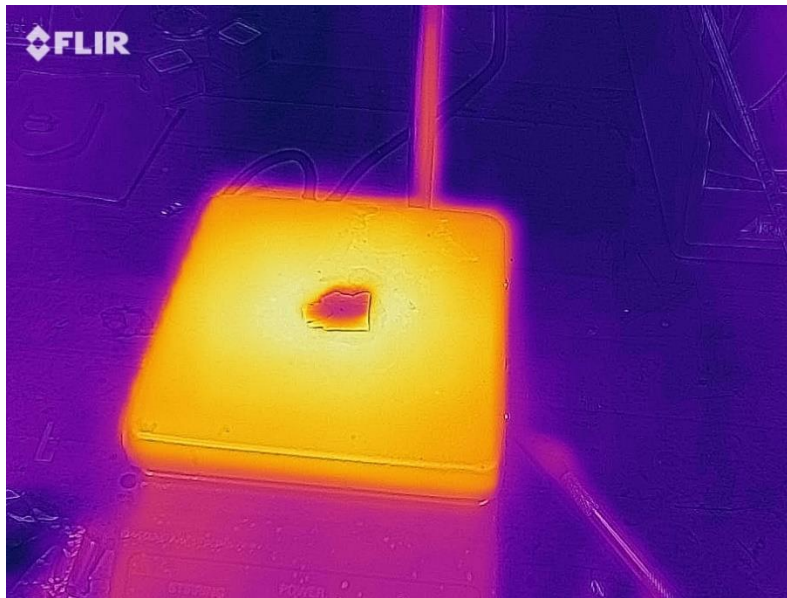
Figure 32: CoO-ATO XP0177 membrane on a hot plate.
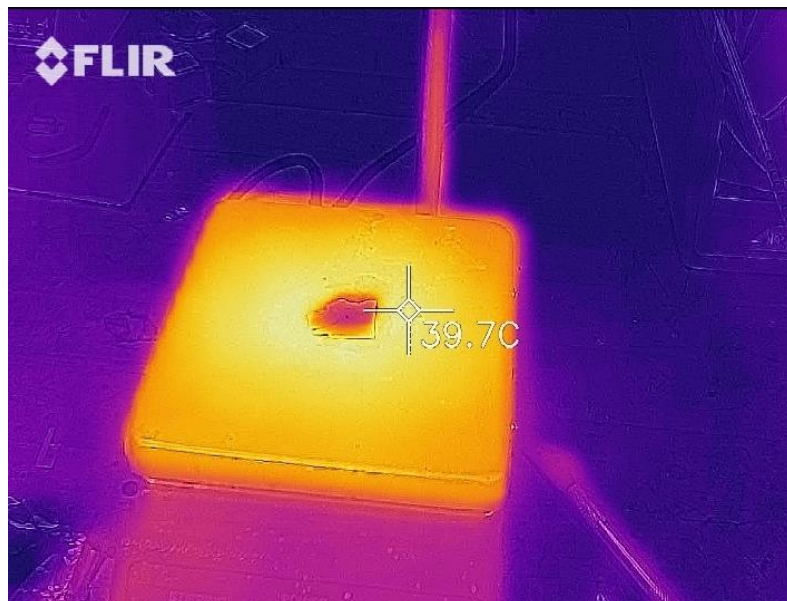
Figure 33: This is the same image as Figure 18 with the hot plate set to 39.7°C.
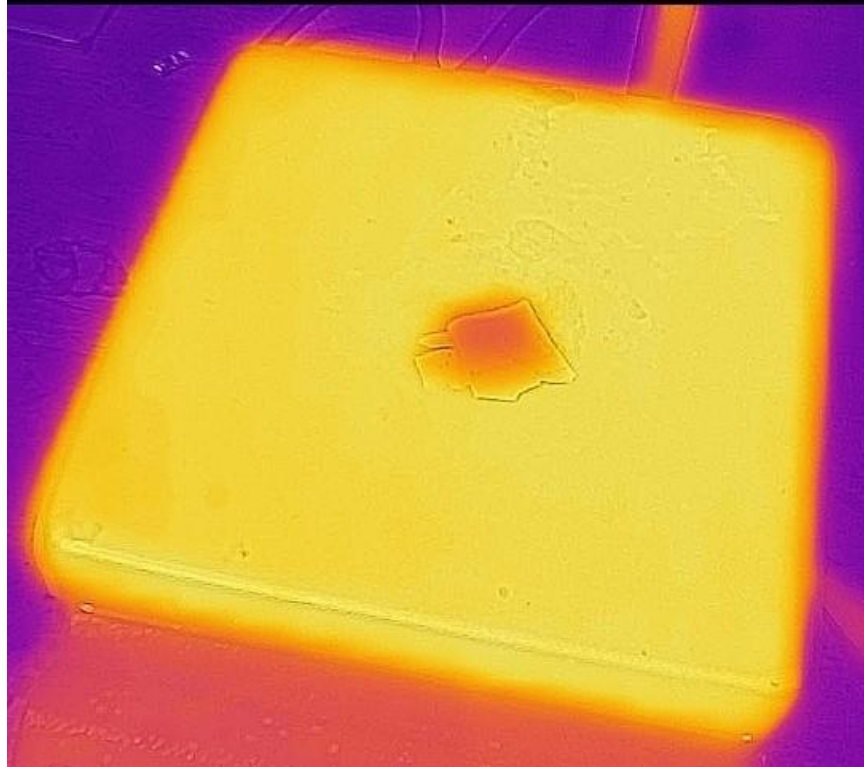
Figure 34: CoO ATO membrane on a hot plate after 5 minutes
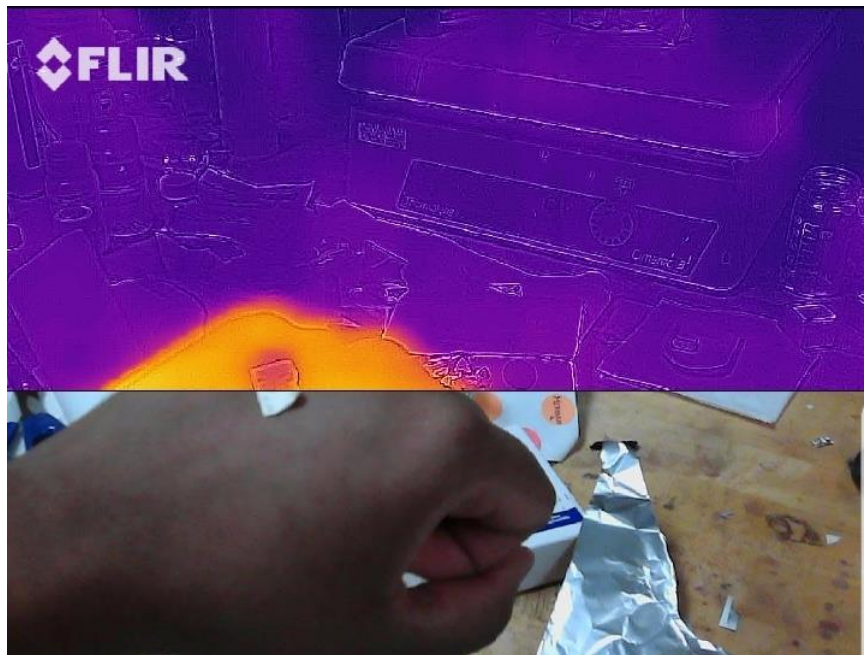
Figure 35: CoO ATO XP0177 membrane on hand

5.5. Results

Three orientations of fibers mesh were tested:

1. Random orientation fiber mesh using a stationary collector.

2. Parallel orientation, and a perpendicular orientation of the fibers mesh with respect to the source using a rotary collector.

XP0177 membranes were tested with random, parallel, and perpendicular orientations. XP0177 - CoO ATO composite membranes were tested with a random orientation.

Different orientations showed a signignificantly different behavior of the polyimide membranes. All the samples show a maximum stress increase of 4 to 5 times, depending on the different structures tested. The samples with a parallel orientation reached the highest max stress at 5.4 N/mm², then the perpendicular orientation at 3.9 N/mm², and finally, the random orientation fibers at 3.9 N/mm².

The results (figure 19) show that the electrospinning process is necessary to improve the polymers' tensile properties. The incorporation of external elements like CoO ATO influences the stress properties in the fibers minimally. It allows for external modifications depending on the final purpose of the product. Tensile testing the different alignments of the fibers plays an essential role in understanding the elasticity of the material. The dog bone shaped cut was used to prepate samples for tensile testing. Sinch this shape is longer in one direction, the samples from the parallel fiber mesh are longer than perpendicular fiber mesh, showing in the strain and stress properties. While the alignment shows an improvement in the stress compared to the random fibers, it becomes detrimental for the strain properties. The shorter length fibers in the perpendicular fiber mesh orientation fail at the lowest strain.

Table 6: Tensile test results for the super elastic fibers [66]

Samples	Stress (N/mm^2) Average Break	Strain (%) Average Break	Stress (N/mm^2) Average Max	Strain (%) Average Max
XP0177 thin film	0.87 ± 0.05	1057.68 ± 71.88	1.04 ± 0.11	641.64 ± 19.28
XP0177 fibers random	3.59 ± 0.62	444.28 ± 43.60	3.91 ± 0.51	436.68 ± 46.49
XP0177 fibers perpendicular	3.33 ± 0.90	171.40 ± 49.98	3.94 ± 0.75	161.88 ± 49.98
XP0177 fibers parallel orientation	4.88 ± 0.52	208.13 ± 23.39	5.40 ± 0.42	202.79 ± 23.15
XP0177 –CoO ATO fibers random orientation	5.18 ± 0.68	310 ± 32.48	2.57 ± 0.32	789.897 ± 56

The parallel fibers appeared to be pre-stretched due to the whipping action seen when the fibers are collected on the collector plate, which also decreases the total strain. The random orientation fibers show impressive mechanical properties with maximum stress that just lags the best performing fiber. Still, it leads the strain by almost doubling any other fiber tested and the closest to the undoped fiber.
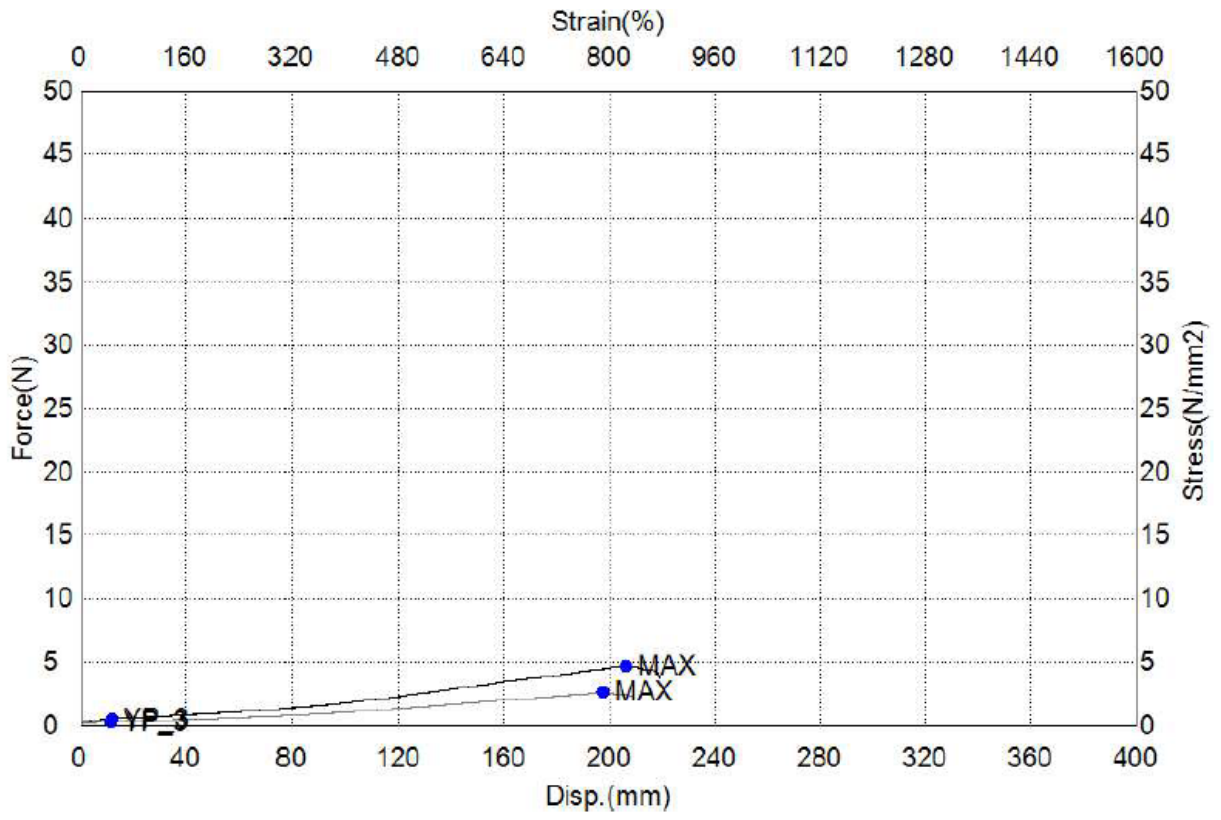
Figure 36: Tensile test for 2% CoO ATO-XP0177 Polyimide
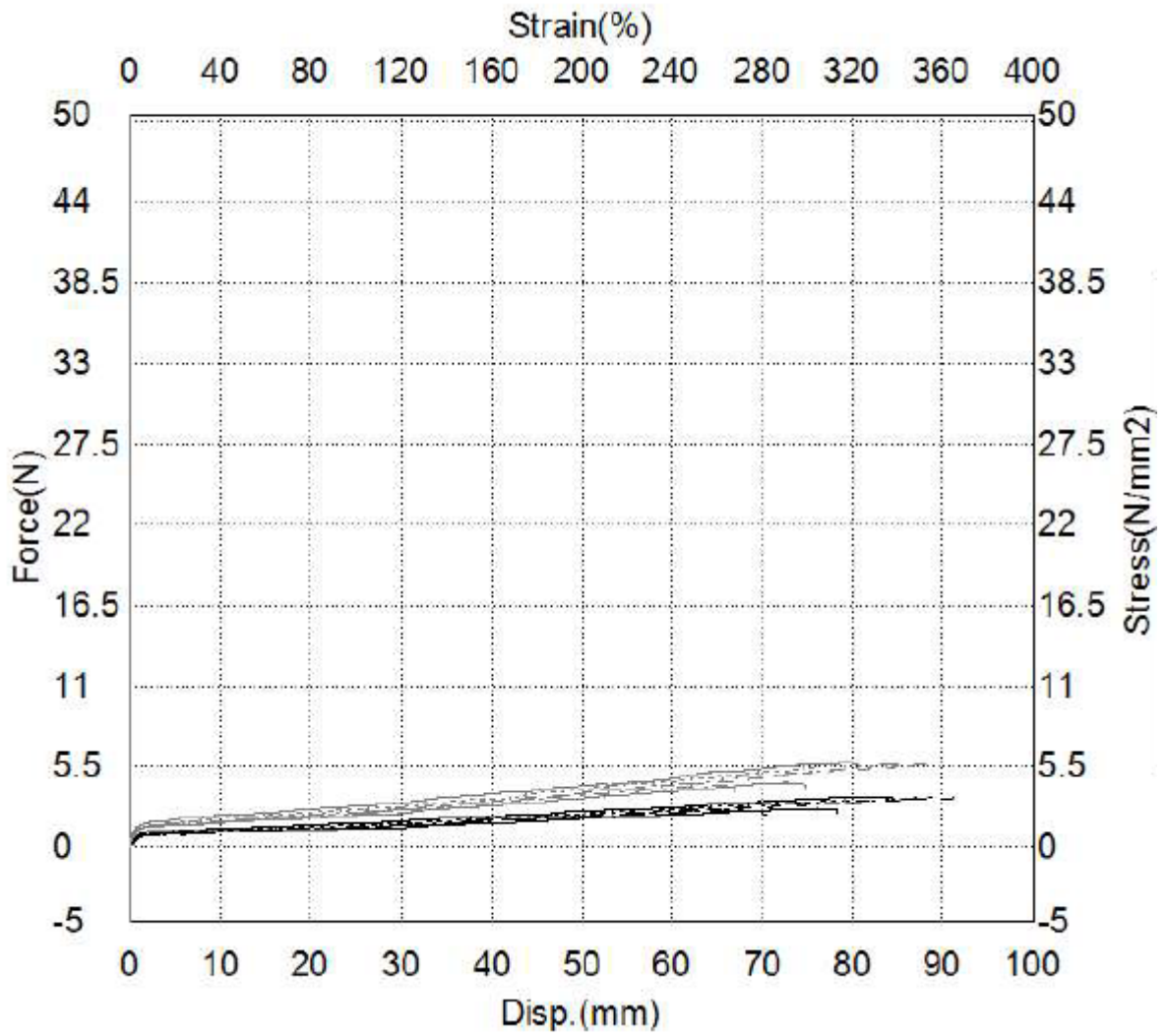
Figure 37: Tensile test 2 for 2% CoO ATO-XP0177 Polyimide

Chapter 6: Summary of Findings

Summary of findings for each application is listed below.

6.1. CoO-ATO Nanofibers on Solar Cells

The antimony tin oxide and cobalt oxide composite are electrospun into fiber membranes using two polymers, polystyrene and a novel polyimide (XP0177).

The fibers spun with polystyrene are coated on a solar cell whose ARC (anti-reflective coating) has been stripped off. This modified structure has improved solar cell performance. The short circuit current reading under sunlight improved by 2.13 mA/cm.

The open-circuit voltage (V_{OC}) measurements are obtained under standard AM1.0 solar spectrum measurements provided. The V_{OC} measurements are 400 mV, 420 mV and 430mV for a solar cell with no ARC, as bought solar cell and CoO ATO solar cell.

Membranes on solar cells have a workable temperature up to 378.6℃, as shown from the TGA results indicating that the membranes' workable temperature is 378.6℃ and that the fiber disintegrates beyond that.

Under AM 1.0 conditions, solar cells with CoO-ATO nanofiber coating have an efficiency of 7.24%. Solar cells with ARC coating are noted to be 5.6% efficient. Thus the increase in efficiency is 29%. The efficiency of the as-is solar cell is 7.06%. The nanofiber coated solar cell is 3% more efficient than the as-is solar cell. Under direct sunlight, 20% increase in current density is noted.

6.2. Super-elastic CoO-ATO Nanofiber Membrane as a Thermal Sheath

Cobalt oxide- antimony tin oxide fibers were electrospun with a novel super elastic polyimide (XP0177). They were tensile tested to test the stress and strain of the fibers. The XP0177 – CoO ATO fiber membrane could stretch to 2.5 times its size at 2.57 N/mm^2. The XP0177 – CoO ATO composite fiber membrane's elastic nature decreased compared to the undoped XP0177 polyimide fiber membrane. The infrared sheath property of the membrane was demonstrated successfully.

Chapter 7: Conclusion and Future Work

For the first time, a novel ferromagnetic metal oxide CoO ATO in a polymeric composite in the form of a fiber membrane has been proven to improve the efficiency of solar cells. A CoO ATO anti-reflective coating for solar cells by using electrospinning, a quick fabrication process was successfully developed. This study paves a way to fulfill the requirements of low cost and low energy consumption process for high-efficiency PVs. This work offers a novel approach to enhance optical and IR shielding properties by improving the efficiency of a solar cell.

The capabilities of CoO ATO are further demonstrated in a composite with a novel super elastic polyimide as a flexible infrared sheath. This polymer, when electrospun in its pure form, is extremely elastic and has potential. The super-elastic infrared sheath was tested for its elasticity and proven to be very stretchable.

Fabricating of the XP0177-CoO ATO composite fiber membrane as a sew-able textile may be considered for applications in the military and promoting stealth. This membrane can be investigated to be used as an antireflecting coating for aerospace vehicles as they are prone to damage by infrared radiation and imaging. A long-term goal of this research is to produce a membrane that can be used as a glove on devices. Large-scale production into a sew-able textile may be investigated. Clothing may be fabricated from the textile.

Investigating the CoO ATO fiber membrane as an intermediate layer in a solar cell to enhance the absorption of photons could be explored. When the processing or manufacturing does not involve more than 378.6C, this ferromagnetic metal oxide polymeric composite antireflecting fiber coating can find an application in most optical device manufacturing. A solar cell

manufacturing process can incorporate this membrane in the end of the processing temperature

does not exceed 378.6.

References

[1] S. P. Mahulikar, H. R. Sonawane and G. A. Rao, "Infrared signatures studies of aerospace vehicles," *Progress in Aerospace Sciences,* pp. 218-245, 2007.

[2] S.-M. Jeong, J. Ahn, Y. K. Choi, L. Taekyung, K. Seo, H. Taekuk , G. H. Choi, H. Kim, B. W. Lee, S. Y. Park and S. Ju, "Development of a wearable infrared shield based on a polyurethane–antimony tin oxide composite fiber," *NPG Asia Materials,* vol. 12, p. 32, 24 April 2020.

[3] B. D. Richard, "Thermal Infrared Reflective Metal Oxide Sol-Gel Coatings for Carbon Fiber Reinforced Composite Structures," *Scholar Commons,* January 2013.

[4] W. Zhang, G. Xu, R. Ding, K. Duan and J. Qiao, "Nacre biomimic design- a possible approach to prepare low infrared emissivity composite coatings," *Material Science Eng: C,* vol. 33, pp. 99-102, 2013.

[5] D. Zabekatis, M. Dinderman and P. Schoen, "Metal Coated cellulose fibers for use in composites applicable to microwave technology," *Advance Materials,* vol. 17, pp. 734-738, 2005.

[6] H. Yu, G. Xu, X. Shen, X. Yan and C. Cheng , "Low infrared emissivity of poly-urathane/Cu Composite Coatings.," *Applied Surf. Sci.,* vol. 255, pp. 6077-6081, 2009.

[7] C. C. Yang, Y. J. Gung, W. C. Hung, T. Ting and K. Wu, "infrared and microwaveabsorbing properties of baTiO3/Polyaniline and BaFe12O19/Poly aniline composites," *Compos Sci Technology,* vol. 70, pp. 466-471, 2010.

[8] Priya Sanjay, "With 2,245 MW of Commissioned Solar Projects, World's Largest Solar Park is Now at Bhadla," *Clean Energy news and insights,* MAr 19, 2020.

[9] Zhang Tian-Hui, Piao Ling Yu, Zhao Su-Ling, Xu Zheng, Wu Qian and Kong Chao, "Chinese physical society and IOP Publication," *Application of Tio2 with Different structures in solar cells,* 2012.

[10] J. Q. Xi, M. Schubert, J. K. Kim, E. F. Schubert, M. Chen, S.-. Y. Lin, W. Liu and J. A. Smart, "Optical thin-film materials with low refractive index for broadband elimination of Fresnel reflection," *Nature Photonics,* vol. 1, pp. 176-179, 2007.

[11] P. Buskens, M. Burghoorn, M. C. D. Mourad and Z. Vroon, "Antireflective Coatings for Glass and Transparent Polymers," *Langmuir,* pp. 6781-6793, 2016.

[12] A. Maxim, S. Sadyk, D. Aydarkhanov, C. Surya, A. Ng, Y. H. Hwang, T. S. Atabaev and A. Jumabekov, "PMMA Thin Film with Embedded Carbon Quantum Dots for Post-Fabrication Improvement of Light Harvesting in Perovskite Solar Cells," *nanomaterials,* vol. 10, no. 2, 2020.

[13] F. Fesharaki, A. Jooshesh, V. Bahrami-Yekta, M. Mahtab, T. Tiedje, T. E. Darcie and R. Gordon, "Plasmonic Antireflection Coating for Photoconductive Terahertz," *ACS Photonics,* vol. 4, pp. 1350-1354, 2017.

[14] Y. F. Makableh, M. Al-Fanidi, M. Khasawneh and C. Tavares, "Comprehensive design analysis of ZnO anti-reflection nanostructures for Si solar cells," *Elsevier,* pp. 1-9, 2018.

[15] M. Devisetty subramanyam, "Fabrication and Comparison of Electrospun Cobalt Oxide-antimony Doped Tin Oxide (CoO-ATO) Nanofibers Made with PS D-limonene and PS Toluene," *Electronic Thesis and Dessertation,* 2014.

[16] Y.-L. e. a. Chen, "Light Scattering and Enhanced Photoactivities of Electrospun Titania Nanofibers," *Journal of Physical Chemistry,* vol. 116, no. 5, pp. 3857-3865, 2012.

[17] S. B. Khan, H. Wu, C. Pan and Z. Zhang, "A Mini Review: Antireflective Coatings Processing Techniques, Applications and Future Perspective," *Research reviews: Journal of Material Science,* vol. 5, no. 4, 2017.

[18] J. w. e. a. Leem, "Broadband and omnidirectional highly-transparent coverglasses coated with biomimetic moth-eye nanopatterned polymer films for solar photovoltaic system applications," *Solar Energy Materials and Solar Cells,* vol. 134, pp. 45-53, 2015.

[19] e. a. Park. S.C., "Fabrication and characterization of moth-eye mimicking nanostructured convex lens," *Microelectronic Engineering,* vol. 158, pp. 38-40, 2016.

[20] J. e. a. Hartgernik, "Self-Assembly and Mineralization of Peptide-Amphiphile Nanofibers," *Science,* vol. 294, no. 5547, pp. 1684-1688, 2000.

[21] S. e. a. Paramonov, "Self-Assembly of Peptide−Amphiphile Nanofibers: The Roles of Hydrogen Bonding and Amphiphilic Packing," *Journal of the americal Chemical Society,* vol. 128, no. 22, pp. 7291-7298, 2006.

[22] C. J. e. a. Ellison, "Melt blown nanofibers: Fiber diameter distributions and onset of fiber breakup," *Polymer,* vol. 48, pp. 3306-3316, 2007.

[23] M. A. e. a. Hassan, "Fabrication of nanofiber meltblown membranes and their filtration properties," *Journal of Membrane Science,* vol. 4, no. 27, pp. 336-44, 2013.

[24] S. e. a. Sinha-Ray, "Pool boiling of Novec 7300 and DI water on nano-textured heater covered with supersonically-blown or electrospun polymer nanofibers," *International journal of heat and Mass transfer,* vol. 106, pp. 482-490, 2017.

[25] S. e. a. Sinha Ray, "Swing-like pool boiling on nano-textured surfaces for microgravity applications related to cooling of high-power microelectronics," *NPJ Microgravity,* vol. 3, pp. 1-9, 2017.

[26] S. e. a. Sinha-Ray, "Solution Blowing of Soy Protein Fibers," *Biomacromolecules,* vol. 12, no. 6, pp. 2357-2363, 2011.

[27] M. W. e. a. Lee., "Solution-Blown Core–Shell Self-Healing Nano- and Microfibers," *ACS Applied Material Interfaces,* vol. 8, no. 7, pp. 4955-62, 2016.

[28] K. Bhilal and e. al., "Direct Blow-Spinning of Nanofibers on a Window Screen for Highly Efficient PM2.5 Removal," *Nano Letters,* vol. 17, no. 2, pp. 1140-1148, 2017.

[29] H. Wang and e. al., "Direct Blow Spinning of Flexible and Transparent Ag Nanofiber Heater," *Advance Material Technology,* vol. 4, 2019.

[30] T. C. M. Julien and e. al., "Ultrasoft polycarbonate polyurethane nanofibers made by electrospinning: Fabrication and characterization," *Polymer Engineering and Science,* vol. 59, no. 4, pp. 838-45, 2019.

[31] J. W. Leem, H. K. Lee, D. H. Jun, J. Heo, W.-K. Park and J. S. Yu, "Electrochemically synthesized broadband antireflective and hydrophobic GaOOH nanopillars for III-V InGaP/GaAs/Ge triple-junction solar cell applications," *Optics Express,* vol. 22, no. 52, pp. A328-A334, 2014.

[32] L. Ye, Y. zhang, X. Zhang, T. Hu, R. Ji, B. Ding and B. Jiang, "Sol–gel preparation of SiO2/TiO2/SiO2–TiO2 broadband antireflective coating for solar cell cover glass," *Solar Energy MAterials and Solar Cells,* vol. 111, pp. 160-164, April 2013.

[33] G. Dingemans and W. M. M. Kessels, "Status and prospects of Al2O3-based surface passivation schemes for silicon solar cells," *Journal of Vacuum Science & Technology,* 2012.

[34] J. C. Sarker, R. Vasan, Y. Makableh, S. Lee, A. Nusir and M. Manasreh, "Enhanced performance of surface modified InAs quantum dots solar cell by a sol–gel grown tantalum pentoxide antireflection coating," *Solar Energy Materials and Solar Cells,* vol. 127, 2014.

[35] B. C. Chakravarty, P. N. Vinod, S. N. Singh and B. R. Chakraborty, "Design and simulation of antireflection coating for application to silicon solar cells," *Solar Energy Materials and Solar Cells,* vol. 73, no. 1, pp. 59-66, 2002.

[36] T. R. Prabhu, "Airworthiness Certification of Fe-Si3N4-graphite Brake Composites for Military Aircraft," *Tribology in industry,* vol. 37, no. 4, pp. 491-499, 2015.

[37] S. Funahashi, T. Nakamura, K. Kageyama and H. Leki, "Monolithic oxide–metal composite thermoelectric generators for energy harvesting," *Journal of applied Physics,* vol. 109, no. 12, 2011.

[38] P. Suresh Kumar , J. Sundaramurthy, S. Sundarrajan, V. Jagadeesh Babu, G. Singh, S. I. Allakhverdiev and S. Ramakrishna, "Hierarchical electrospun nanofibers for energy harvesting, production and environmental remediation," *Energy and Environmental Science,* vol. 7, no. 10, pp. 3192-3222, 2014.

[39] "Laser ablation of CFRP using picosecond laser pulses at different wavelengths from UV to IR," *Physics Procedia,* vol. 12, no. B, pp. 292-301, 2011.

[40] D. Micheli, C. Apollo, R. Pastore, R. B. Morles, S. Lorenzi and M. Marchetti, "Nanostructured composite materials for electromagnetic interference shielding applications," *Acta Astronautica,* vol. 69, no. 9-10, pp. 747-757, 2011.

[41] A. Gupta, M. Cizmecioglu, D. Coulter, R. H. Liang, A. Yavrouian, F. D. Tsay and J. Moacanin, "The mechanism of cure of tetraglycidyl diaminodiphenyl methane with diaminodiphenyl sulfone," *Applied Polymer Science,* vol. 28, 1983.

[42] J. Liu, Z. Guo, F. Meng, Y. Jia, T. Tuo, M. Li and J. Liu, "Novel Single-Crystalline Hierarchical Structured ZnO Nanorods Fabricated via a Wet-Chemical Route: Combined High Gas Sensing Performance with Enhanced Optical Properties," *Crystal Growth and Design,* vol. 9, no. 4, pp. 1716-1722, 2009.

[43] V. Geraldo, L. V. Scalvi, P. N. L. Filho and M. Santos, "Drude's model calculation rule on electrical transport in Sb-doped SnO2 thin films, deposited via sol–gel," *Journal of Physics and Chemistry of Solids,* vol. 67, no. 7, pp. 1410-1415, 2006.

[44] I. Saadedin, B. Pecquenard, J. P. Manaud, R. Decourt, C. Labrugere, T. Buffeteau and G. Campet, "Synthesis and characterization of single- and co-doped SnO2 thin films for optoelectronic applications," *Applied Surface Science,* vol. 253, no. 12, pp. 5240-5249, 2007.

[45] T. Tsuzuki, K. Pethick and P. G. McCormick, "Synthesis of CaCO3 Nanoparticles by Mechanochemical Processing," *Journal of Nanoparticle Research,* pp. 375-380, 2000.

[46] S. e. Music, "Formation of Chromiafrom amorphous chromiumhydroxide," *Croatia Chemica Acta,* vol. 72, no. 4, pp. 789-802, 1999.

[47] X. Xang, Y. Hu, L. Song, W. Xing, H. D. Lu, P. Lv and G. Jie, "Effect of antimony doped tin oxide on behaviors of waterborne polyurethane acrylate nanocomposite coatings," *Surface and coatings Technology,* vol. 205, no. 7, pp. 1864-1869, 2010.

[48] H. Bisht, H. T. Eun, A. Mehrtens and M. A. Aegerter, "Comparison of spray pyrolyzed FTO, ATO and ITO coatings for flat and bent glass substrates," *Thin solid films,* vol. 351, no. 1-2, pp. 109-114, 1999.

[49] C. Naghvi, I. L. Marce, J. Dupont and J. M. Tarascon, "On the electrochromic properties of antimony–tin oxide thin films deposited by pulsed laser deposition," *Solid State Ionics,* vol. 156, pp. 463-474, 2003.

[50] R. Gordon, " Criteria for choosing transparent conductors," *MRS bulletin ,* 2000.

[51] S. Ramasamy, C. Shanthi and P. Subramanian, "Investigations on the Optical Properties of Undoped, Fluorine Doped and Antimony Doped Tin Oxide Films," *Crystal Research and Technology,* 1999.

[52] S. Ngasinlapasaithian, S. Yoshikazu, S. Thammanoon and Y. Susumu, "Doubled layered ITO/SnO2 conducting glass for substrate of dye-sensitized solar cells," *Solar energy materials and solar cells,* vol. 90, no. 14, pp. 2129-2140, 2006.

[53] I. Chambuleyron and E. Saucedo, "Properties of chemically sprayed SnO2 antireflecting films on Si solar cells," *Solar Energy Materials,* vol. 1, no. 3-4, pp. 299-311, 1979.

[54] I. A. Zhurbina, O. I. Tsetlin and V. Y. Timoshenko, "Optical generation of free charge carriers in thin films of tin oxide," *Semiconductors,* vol. 45, no. 2, pp. 236-240, 2011.

[55] Y. N. Muraoka, N. Takubo and Z. Hiroi, "Photoinducedconductivity in tin dioxide thin films," *Journal of applied physics,* vol. 105, no. 10, 2009.

[56] M. K. Singh, M. C. Mathpal and A. Agarwal, "Optical properties of quantum dotssynthesized by Laser ablation in liquid," *Chemical Physics Letters,* vol. 536, pp. 87-91, 2012.

[57] E. Shanthi, "Electrical and optical-properties of tin oxide-films doped with F and (SB+F)," *Journal of Applied Physics,* vol. 53, no. 3, pp. 1615-1612, 1982.

[58] B. Stjerna, E. Olsson and C. G. Granqvist, "Optical and electrical properties of radio frequency sputtered tin oxide films doped with oxygen vacancies, F, Sb, or Mo," *Journal of Applied Physics,* vol. 76, no. 6, p. 1397, 1994.

[59] A. E. Shalan, T. Oshikiri, S. Narra , M. M. Elshanawany, K. Ueno, H.-P. Wu, K. Nakamura, X. Shi, E. W.-G. Diau and H. Misawa, "Cobalt Oxide (CoOx) as an Efficient Hole-Extracting Layer for High-Performance Inverted Planar Perovskite Solar Cells," *ACS Applied Material Interfaces,* vol. 49, no. 8, pp. 33592-33600, 17 November 2016.

[60] Y. Xie, K. Lu, J. Duan, Y. Jiang, L. Hu, T. Liu, Y. Zhou and B. Hu, "Enhancing Photovoltaic Performance of Inverted Planar Perovskite Solar Cells by Cobalt-Doped Nickel Oxide Hole Transport Layer," *American Chemical Society,* vol. 10, no. 16, pp. 14153-14159, 2018.

[61] S. Wang, B. Zhang, D. Feng, Z. Lin, J. Zhang, Y. Hao, X. Fan and J. Chang, "Achieving high performance and stable inverted planar perovskite solar cells using lithium and cobalt co-doped nickel oxide as hole transport layers," *Journal ofMaterial Chemistry ,* vol. 7, no. 30, pp. 9270-9277, 2019.

[62] J. H. Lee, Y. W. Noh, I. S. Jin, S. H. Park and J. W. Jung, "Efficient perovskite solar cells with negligible hysteresis achieved by sol–gel-driven spinel nickel cobalt oxide thin films as the hole transport layer," *Journal of Material Chemistry,* vol. 7, no. 24, pp. 7288-7298, 2019.

[63] P.-H. Lee, B.-T. Li, C.-F. Lee, Y.-C. Huang and W.-F. Su, "High-efficiency perovskite solar cell using cobalt doped nickel oxide hole transport layer fabricated by NIR process," *Solar Energy Materials and Solar Cells,* vol. 208, 2020.

[64] A. Amri, X. Duan, C. -. Y. Yin, Z. T. Jiang, M. M. Rahman and T. Pryor, "Solar absorptance of copper–cobalt oxide thin film coatings with nano-size, grain-like morphology: Optimization and synchrotron radiation XPS studies," *Applied Surface Science,* vol. 275, pp. 127-135, 2013.

[65] Y. Jiang, "Synthesis and characterization of alpha-Fe2O3@ATO nanocomposite particles," *Surface Review Particles,* vol. 15, no. 5, pp. 545-550, 2007.

[66] A. Rivera Nicholls, "Formulation to Application: Thermomechanical Characterization of Flexible Polyimides and The Improvement of Their Properties Via Chain Interaction," *GRADUATE THESES AND DISSERTATIONS, scholar commons,* 2019.

[67] Y. e. a. Tang, "Highly reflective nanofiber films based on electrospinning and their application on color uniformity and luminous efficacy improvement of white light-emitting diodes," *Optics Express,* vol. 25, no. 17, pp. 20598-20611, 2017.

[68] K. C. Sahoo, Y. Li and E. Y. Chang, "Shape Effect of Silicon Nitride Subwavelength Structure on Reflectance for Silicon Solar Cells," *IEEE Transactions on Electron Devices,* vol. 57, no. 10, pp. 2427-2433, 2010.

[69] R. R. Khan, "Modeling, Simulation and Characterization of Optoelectronic Properties of 2D-3D CoO ATO nanostructures," *Graduate Thesis and Dissertations,* 2017.

[70] K. Abe, Y. Sanada and T. Morimoto, "Anti-Reflective Coatings for CRTs by Sol-Gel Process," *Journal of Sol-Gel Science and Technology,* pp. 151-156, 2001.

[71] A. R. Plotkin, M. K. Toupin, C. B. Gillum, R. J. Rancatore, T. Yang and M. Diego, "Solar

Receiver Steam Generator Design for the Ivanpah Solar Electric Generating System," *ASME

2011 Power Conference ,* pp. 523-529, July 2012.

Appendices

Appendix A: Copyright Permission from Alejandro Rivera Nicholls

The permission below is for the use of material in chapter 2 and chapter 5.

Permission

Rivera Nicholls, Alejandro <ariveranicho@usf.edu>
Sun 4/4/2021 2:59 PM
To: Devisetty Subramanyam, Manopriya <manopriya@usf.edu>
To whom may it concern,

I, Alejandro Rivera Nicholls, as a copyright holder of "**Formulation to Application: Thermomechanical Characterization of Flexible Polyimides and The Improvement of Their Properties Via Chain Interaction**" published in USF Sholar commons ETD, authorize Manopriya Devisetty Subramanyam to use images and data from the chapter "Flexible Polyimide Nanofibers Made by Electrospinning: Fabrication and Characterization" in her thesis and dissertation work.

Sincerely,

Alejandro Rivera Nicholls